From Grunts to Lexicons: Emergent Language from Cooperative Foraging

Anonymous authors
Paper under double-blind review

Abstract

Language is a powerful communicative and cognitive tool. It enables humans to express thoughts, share intentions, and reason about complex phenomena. Despite our fluency in using and understanding language, the question of how it arises and evolves over time remains unsolved. A leading hypothesis in linguistics and anthropology posits that language evolved to meet the ecological and social demands of early human cooperation. Language did not arise in isolation, but through shared survival goals. Inspired by this view, we investigate the emergence of language in multi-agent Foraging Games. These environments are designed to reflect the cognitive and ecological constraints believed to have influenced the evolution of communication. Agents operate in a shared grid world with only partial knowledge about other agents and the environment, and must coordinate to complete games like picking up high-value targets or executing temporally ordered actions. Using end-to-end deep reinforcement learning, agents learn both actions and communication strategies from scratch. We find that agents develop communication protocols with hallmark features of natural language: arbitrariness, interchangeability, displacement, cultural transmission, and compositionality. We quantify each property and analyze how different factors, such as population size, social dynamics, and temporal dependencies, shape specific aspects of the emergent language. Our framework serves as a platform for studying how language can evolve from partial observability, temporal reasoning, and cooperative goals in embodied multi-agent settings. We will release all data, code, and models publicly.

1 Introduction

The evolution of human language remains a central open question in science. While humans fluently use and understand language, its origins are still debated. One influential view proposes that language emerged through cooperative interaction under partial observability (Sterelny, 2012; Tomasello, 2010; Nowak et al., 2000; Christiansen & Kirby, 2003; Nowak & Komarova, 2001). Rather than functioning as an abstract code, language is understood as a tool shaped by social use and shared goals (Wittgenstein, 2009; Wagner et al., 2003). Although direct evidence from early stages is unavailable, multi-agent simulations offer a way to examine how ecological and social conditions might have shaped language (Cangelosi & Parisi, 2012; Kirby et al., 2014; Lazaridou et al., 2017; 2018).

Prior work on Emergent Communication (EC) has primarily focused on referential games (RG), where a speaker conveys task-relevant information to a listener over a limited communication channel (Lazaridou et al., 2017; Lewis, 2008; Kharitonov et al., 2019; Gualdoni et al., 2024). These settings have advanced our understanding of symbol grounding and compositionality, but often impose simplifying assumptions: agents are limited to unidirectional communication (Galke et al., 2022), operate in fixed speaker-listener roles, and perform disembodied tasks with passive input processing and no active interaction with the environment. Even recent extensions to population-based learning (Dubova & Moskvichev, 2020; Dubova et al., 2020; Kim & Oh, 2021; Chaabouni et al., 2022; Michel et al., 2023) typically decouple communication from physical behavior. Such setups diverge from the ecologically grounded, socially interdependent, and embodied conditions under which human language likely evolved (Tomasello, 2010; Dessalles, 2007). The pioneering work that integrates embodiment into EC (Mordatch & Abbeel, 2018) reveals richer aspects of emergent language, including the co-learning of physical and linguistic behavior and the use of bodily actions as implicit communication. However, it does not incorporate biologically plausible decentralized learning,

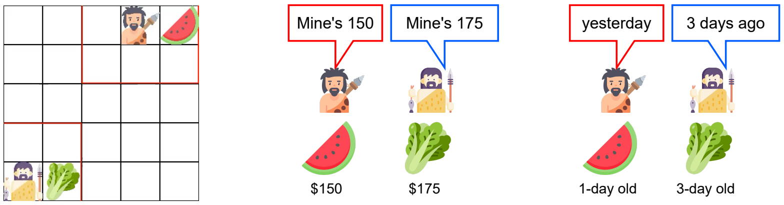

(a) Foraging Games (b) *ScoreG* (c) *TemporalG*

Figure 1: **An Overview of Foraging Games.** (a) Two agents operate in a 5×5 partially observable grid world. Each agent can observe a 3×3 grid centered on itself. The two agents are required to pick up the goal items simultaneously. (b) *ScoreG* game: Two items are assigned random scores; each agent observes only one score, and both must pick up the higher-scoring item to succeed in an episode. This game is designed to encourage agents to communicate about items' scores. (c) *TemporalG* game: Two items spawn at random times, each observed by only one agent. Agents must collect them in chronological order, encouraging communication about time.

agent heterogeneity, or population structure, limiting its ability to support broader studies of EC in embodied settings.

Following this line of work (Mordatch & Abbeel, 2018), we introduce Foraging Games (FG), a multi-agent framework designed to reflect more realistic ecological and cognitive constraints that may have shaped early human language (Dessalles, 2007; Tomasello, 2010). FG supports bidirectional communication. Agents are trained to jointly learn both physical action and communication, as early humans likely did during cooperative foraging. The environment enforces embodiment: agents must explore, observe, and act within a dynamic and partially observable world that they can influence. Moreover, each agent interacts with a population of diverse partners, facilitating the study of generalization to new partners, dialect formation, and cultural transmission (Kim & Oh, 2021; Rita et al., 2022; Michel et al., 2023).

Specifically, we formulate FG as a partially observable grid world in which agents must complete multi-step games as shown in Fig. 1. Success depends not only on taking effective actions, but also on communicating what they see and know. It includes two games: (1) collecting the most valuable item with a partner, which encourages communication about items' scores and locations, and (2) picking up items in a specific order with a partner, which requires communication about when items were seen. Each agent has deep neural network modules for perception, memory, and policies to translate internal representations into actions and messages. Agents communicate through discrete messages drawn from a finite set of learnable vocabulary exchanged at each time step. They are trained independently using Proximal Policy Optimization (PPO) (Schulman et al., 2017), with no shared parameters, or gradients, reflecting the personalized and decentralized nature among agents.

With this framework in place, we aim to provide answers to the following questions: **(Q1)** What properties does emergent communication have when it arises in embodied, interactive, and collaborative agents? **(Q2)** Do agents truly understand the language they use, and what drives the emergence of a shared language when the same agent acts as both speaker and listener? **(Q3)** How do population size and social dynamics affect the emergent language? **(Q4)** Can agents refer to spatial and temporal events through their language? **(Q5)** Can agents communicate implicitly through non-verbal behaviors, such as body movements?

Empirically, we find that agents achieve a success rate (SR) above 95% across all games. Although two trained agents perform well when paired with each other, each fails when paired with a copy of itself at test time, suggesting that an agent understands only its partner's language, not the one it produces. We propose two solutions to this problem. The first is to train a population with more than two agents. We hypothesize that developing a shared language becomes the optimal strategy when agents must communicate with multiple partners. The second is to incorporate self-interaction during training (Dubova & Moskvichev, 2020; Lowe et al., 2020; Charakorn et al., 2023; 2024; Liu et al., 2025a), motivated by the observation that humans can speak to themselves. These solutions encourage agents to comprehend their own messages, promoting convergence on a shared common language and reflecting the property of interchangeability. Since human language develops in populations, we further explore language properties in groups of agents connected via different social structures: fully-connected, ring-structured, and small-world-structured networks. We decode task-relevant information, such as items' positions, scores, and spawn times, from the agents' messages using logistic regression, verifying that the messages are meaningful rather than random. Above-chance decoding accuracy indicates that a language has emerged to communicate item properties. Specifically, agents develop time adverbials (Lipinski et al., 2023) that refer to when past events occurred, along with messages indicating the location of those events. Finally, we show that agents can develop implicit communication (Wang et al., 2025a; Grupen et al., 2022; Dreyer et al., 2025), i.e., gaining information by observing a partner's behavior, when they are unable to send messages.

Our novel contributions are as follows:

1. We introduce Foraging Games, a framework for studying emergent communication that provides ecological and cognitive constraints resembling those faced by early humans, including embodiment, behavior coordination, partial observability, bidirectional communication, and temporal reasoning.

2. We propose a hybrid cross-and-self-play training regime that enhances cultural transmission in weakly-connected social networks: agents that are closer in the training population develop more similar languages than those farther apart.

3. We design a series of tasks in FG that elicit both temporal and spatial displacement in emergent language, which could not arise without embodiment.

2 Related Work

EC offers insights for exploring the processes and pressures that might have shaped the evolution of language (Lazaridou et al., 2017; 2018; Kirby et al., 2014; Chaabouni et al., 2022; Cangelosi & Parisi, 1998; Cangelosi, 2001; Boldt & Mortensen, 2024; Peters et al., 2025; Lazaridou & Baroni, 2020) and the development of more effective representations (Mu & Goodman, 2021; Carmeli et al., 2025; Zion et al., 2024; Denamganai et al., 2024; Yao et al., 2022). Early studies employed evolutionary computation (Cangelosi & Parisi, 1998; Cangelosi, 2001) or Bayesian modeling (Nowak et al., 2000; Kirby et al., 2007) to simulate language emergence and its dynamics. The advent of deep reinforcement learning (DRL) (Mnih et al., 2013; 2015) introduced a more powerful framework for studying EC in realistic, complex settings (Foerster et al., 2016).

Contemporary work often applies DRL to Lewis-style referential games (RG) (Lewis, 2008), where a speaker conveys task-relevant information to a listener through a limited communication channel, typically for target identification or input reconstruction (Zion et al., 2024; Gualdoni et al., 2024; Lipinski et al., 2024; Kharitonov et al., 2019). Because language is inherently social, research has shifted toward population-level studies (Dubova & Moskvichev, 2020; Dubova et al., 2020; Kim & Oh, 2021; Chaabouni et al., 2022; Rita et al., 2022; Michel et al., 2023), examining how social dynamics and population training influence consistency (Dubova & Moskvichev, 2020; Dubova et al., 2020) and dialect formation (Kim & Oh, 2021). However, many resulting frameworks resemble autoencoders (Kingma et al., 2014; Higgins et al., 2017; Ueda & Taniguchi, 2024), treating language as a compressed latent code rather than a flexible medium for real-world coordination.

Recent studies have examined more realistic conditions, such as bidirectional exchange, where agents both send and receive messages (Evtimova et al., 2018; Dubova & Moskvichev, 2020; Dubova et al., 2020; Taillandier et al., 2023; Graesser et al., 2019; Kottur et al., 2017; Nikolaus, 2024), and embodiment (Jain et al., 2019; Patel et al., 2021; Mordatch & Abbeel, 2018; Kajic et al., 2020; Bullard et al., 2020), where agents learn to communicate through interaction with their environment and partners. Only two studies (Mordatch & Abbeel, 2018; Jain et al., 2019) incorporate both. Most embodied EC work (Jain et al., 2019; Patel et al., 2021) prioritizes task performance over analyzing EC itself and omits biologically plausible decentralized training. Another line of research uses EC as a control prompt, outperforming natural language in embodied tasks (Mu et al., 2023), though it is still learned through disembodied RG.

A foundational precursor to our work is (Mordatch & Abbeel, 2018), which studies emergent communication in an embodied multi-agent setting where agents coordinate through discrete symbols while acting in a continuous 2D world. Their work demonstrates the emergence of interpretable vocabularies and analyzes compositional structure under vocabulary-size pressure. Our work builds on this line of research while differing in several key respects. First, their agents share a single policy and rely on a fully differentiable environment that enables backpropagation through joint dynamics, whereas we use decentralized, independently trained agents interacting in a non-differentiable

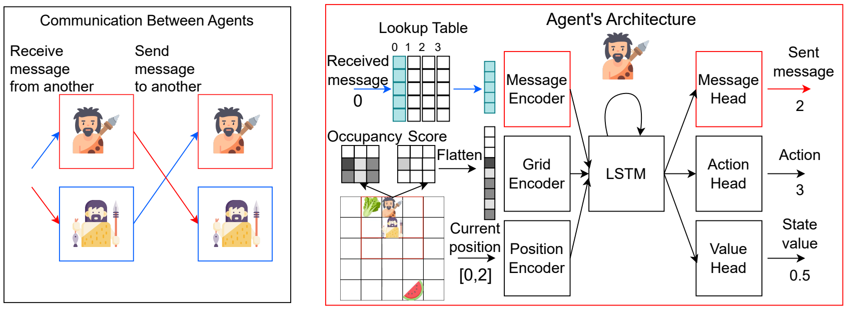

(a) Message Exchange

(b) Architecture Overview

Figure 2: **A graphical overview of our method.** (a) Agents exchange messages at every time step. (b) The neural architecture of a single agent. On the input side, the received integer message is mapped to a real-valued vector via a learnable lookup table and passed through the message encoder. The grid observation and agent position are processed by the grid encoder and position encoder, respectively. The outputs of all three encoders are concatenated and passed to an LSTM module, which maintains temporal memory. On the output side, the message head, action head, and value head produce the next message token, environment action, and estimated state value.

environment, with communication emerging purely from reward signals. Second, they do not examine population-level learning, social-network structure, or cultural transmission dynamics. Third, although they qualitatively analyze compositional symbol reuse, they do not quantify linguistic properties such as compositionality, interchangeability, or displacement—properties we measure explicitly.

3 Foraging Games (FG)

Foraging-style games are used as benchmarks for multi-agent reinforcement learning (MARL) algorithms (Albrecht & Ramamoorthy, 2013; Papoudakis et al., 2021; Yang et al., 2022; Jafferjee et al., 2022; Jaques et al., 2019; Ikram et al., 2021). However, existing environments often assume full observability and are not designed to support the study of emergent communication. We develop our FG, in which decentralized agents share a common goal and must navigate to and simultaneously pick up the goal items to earn equal rewards. Our FG is designed to encourage agents to communicate bidirectionally about their observations. Each agent is provided with only partial knowledge of the environment (e.g., observing only one item). Agents must reach a consensus based on their perspectives by communicating the message from a fixed-size dictionary with learnable embeddings and choosing appropriate actions, where the action space is {move left, move right, move up, move down, and pick up}. FG has two games: *ScoreG* and *TemporalG*. The former is used to investigate four properties of emergent language: **interchangeability** (agents can understand the messages they produce), **arbitrariness** (symbols acquire meaning through social agreement rather than inherent structure), **compositionality** (messages are built from reusable parts reflecting task semantics), and **cultural transmission** (language patterns are passed across agents), under varying population sizes and training regimes. The latter focuses on **displacement**, aiming to determine whether agents' messages encode temporal and spatial information about seen items in the past.

Game 1: *Pickup High Score (ScoreG)* is set in a $2D$ grid world with the size of 5×5, containing 2 items, 2 agents, and a wall, as shown in Fig. 1. The wall refers to the area outside the 5×5 grid. Each grid cell can be occupied by either an agent or an item, but not both simultaneously. Agents cannot move to the wall, the occupied grid cell, or the same grid cell. Each agent receives an observation $\mathbf{o}^{(t)} = (\mathbf{x}^{(t)}, \mathbf{p}^{(t)})$, where $\mathbf{x}^{(t)} \in \mathbb{R}^{3\times3\times2}$ (3 is the receptive field size and 2 refers to two channels). The first channel of the receptive field $\mathbf{x}^{(t)}$ represents an occupancy map: a value of zero indicates that a grid cell contains neither an item nor a wall. The second channel shows the item's score. The receptive field of each agent has its center at the agent and observes the agent's surroundings, delineated as a red box in Fig. 1. To simulate incomplete knowledge, each agent observes the score of one item during an episode. The agent's absolute position in the environment is given by $\mathbf{p}^{(t)} \in \mathbb{R}^2$. The goal item is defined as the item with the highest score. An episode is deemed successful if both agents navigate to and simultaneously pick up the goal item. In this case, they receive a shared positive reward of $+1$; otherwise, they receive a shared negative reward of -1. Additionally, similar to (Wijmans et al., 2020), successful episodes grant both agents a bonus reward r_b based on their efficiency: $r_b = \frac{T_{\max} - T_{\text{total}}}{T_{\max}}$, where $T_{\max} = 10$ is the maximum number of steps allowed per episode, and T_{total} is the total number of steps taken by the agents. The bonus is to encourage the agents to complete the game as soon as possible. To prevent agents from overfitting to specific scores in the *ScoreG* task while still evaluating in-distribution generalization, we use a held-out set of test scores that do not overlap with those seen during training. Specifically, training scores are randomly sampled from the set $\{5, 10, 15, \dots, 250\}$, while test scores are sampled from the disjoint set $\{2, 4, 6, 8, 12, \dots, 248\}$. This setup ensures that test scores lie within the same distributional range as the training scores, while remaining unseen during training. We also include the game variant to unseen item positions in Sec. C.5. To isolate the role of explicit communication, agents are made invisible to one another by default, i.e., a grid cell occupied by another agent appears empty. This design prevents any form of implicit communication through visual cues (Wang et al., 2025a; Grupen et al., 2022; Li et al., 2021; 2024).

Game 2: *Pickup Temporal Order (TemporalG)* Two agents must cooperatively pick up two items by first navigating to and simultaneously collecting the first spawned item, followed by the second. The pickup must occur in the same order as the items appear. The environment follows the same configuration as *ScoreG*, except the agent's observation $\mathbf{x}^{(t)}$ excludes the score channel, and the episode length is limited to $T_{\max} = 20$. Initially, agents are spawned on opposite sides of the grid and remain frozen at time step $t = 1$ to $t = 6$. Subsequently, each item appears at a distinct time step, drawn uniformly from the fixed duration set $\{1, 2, 3, \dots, 6\}$. Each item is guaranteed to appear within at least one agent's receptive field, ensuring it is visible when it spawns. Agents begin moving and attempting to pick up the items only after $t = 6$. Communication is restricted to adjacent grid cells; otherwise, a zero-value message is transmitted. This constraint induces spatial and temporal displacement, compelling agents to retain an event's time and location and later articulate this information once they rendezvous with their partners. Rewards follow the same scheme as in *ScoreG*.

4 Experimental Setting

Embodied Social Agents. As shown in Fig. 2b, each agent in our environment learns both to produce actions and to send and receive discrete messages through a policy trained with PPO (Schulman et al., 2017) (Sec. A.1). For an experiment on unidirectional communication, see Sec. C.2. We denote the overall policy of an agent as $\psi = (\pi, \phi)$, where π is the action policy that selects an environment action, and ϕ is the communication policy that selects a discrete message $\mathbf{m}^{(t)}$ to send. We formulate communication as a sequence of discrete messages. At each time step t, an agent is only allowed to send one discrete message, where each message is represented by a single integer $\mathbf{m}^{(t)} \in \{0, 1, 2, 3\}$. This integer indexes into a lookup table of 4 learnable embeddings (each of dimension 16) in the receiving agent. Each agent maintains its own message lookup table, which is not shared. In other words, upon receiving a message $\mathbf{m}^{(t)}$, the agent retrieves the corresponding message embedding from its own lookup table. We also report results for vocabulary sizes other than the default of 4 in Tab. S5.

All agents share the same neural network architecture but are initialized with independent random parameters. At each time step, the agent receives three inputs: a partial grid observation $\mathbf{x}^{(t)}$, its own position $\mathbf{p}^{(t)}$, and the message $\mathbf{m}^{(t-1)}$ from its partner sent in the previous time step (see Fig. 2a). Each input is encoded separately, using a multi-layer perceptron for the grid, a linear layer for the position, and a multilayer perceptron for the message. The encoded features are concatenated and passed into a long short-term memory network (LSTM) (Hochreiter & Schmidhuber, 1997), which maintains temporal information in a working memory and outputs a hidden state. This hidden state is used to produce three outputs: a distribution over actions, a distribution over messages, and a scalar value estimate used for computing the PPO advantage (Schulman et al., 2016). Both the action and the message are sampled from their respective probability distributions predicted by the agent. The message is used to index into the receiver agent's lookup table, retrieving the corresponding embedding, which is then used by the communication policy ϕ of the receiver agent to produce the message output for the current time step t.

Training Regimes. We train each agent independently using standard single-agent PPO, with no shared parameters or centralized critic. Each agent treats its partner as part of the environment and learns solely from its own experience. Communication policies emerge through interaction and reward, without explicit supervision. This decentralized setup is intentional: it allows agents to specialize, diverge, and adapt to others, enabling us to study how communication protocols evolve under varying population sizes, agent heterogeneity, and connectivity patterns among agents. To investigate how communication strategies emerge and generalize in populations, we explore two training regimes that differ in how agents interact with other partners. These regimes allow us to study the effects of population diversity, message alignment, and exposure to self-produced messages on communication development. **Cross-Play Training (XP):** We define the agent population size as N_{pop}. In each training episode, a pair of agents is randomly sampled from the population to play together. **Cross-Play-and-Self-Play Training (XP+SP):** Motivated by this aspect of inner monologue, humans being able to speak to themselves, in each episode, we randomly select either two distinct agents (Cross-Play, XP) or the same agent twice (Self-Play, SP). Specifically, for each episode, we randomly sample agents i and j such that either $i \neq j$ or $i = j$, where $i, j \in \{1, \ldots, N_{\text{pop}}\}$.

Social Network Structure. We consider several social network structures (Fig. S3): Fully Connected (FC), where every agent interacts with all others; Ring, where each agent interacts only with immediate neighbors; Ring with Cliques (Clq), which adds short-range clusters to the ring; Watts–Strogatz (WS), which rewires a fraction of ring edges to create small-world shortcuts; and Ring with Long-Range Connections (LRC), which augments the ring with distant edges. FC represents the dense baseline. Ring is the sparsest structure while still connected, allowing us to test how communication propagates along long paths. Adding cliques or long-range links (Clq, WS, LRC) reduces social distance and is expected to strengthen language transmission compared to Ring (Sec. B).

Evaluation Metrics on Language Properties. To evaluate linguistic properties in emergent communication, we use three standard metrics and a new metric below. Formal definitions of these metrics are provided in Sec. A.3. Briefly, **Topographic Similarity (*topsim*)** (Brighton & Kirby, 2006; Lazaridou et al., 2018; Kharitonov et al., 2019) measures the structural alignment between message space and semantic space. It is computed as the Spearman correlation between pairwise distances in the message space and the corresponding distances in the semantic space, which reflects the agent's observations and context. **Representational Compositionality (*repcom*) Elmoznino et al. (2025)** quantifies whether semantic representations can be reconstructed from messages using a low-complexity function. Languages achieve higher *repcom* when the mapping function is low-complexity and when it reconstructs the representations accurately, reflecting both simplicity and predictive power. **Language Similarity (*LS*)** (Kim & Oh, 2021; Rita et al., 2022; Michel et al., 2023) measures how similarly two agents communicate in the same situation. It compares the sequences of discrete messages each agent produces and computes the average agreement between them. **Interchangeability (*IC*)** measures whether an agent can understand the language it produces. We define **Self-SR** as the success rate when an agent plays with a copy of itself, and **Cross-SR** as the success rate when paired with a different agent. The overall success rate is denoted as **SR**. *IC* is the ratio of Self-SR to Cross-SR. A high *IC* indicates that agents can better generalize and interpret their own language.

Implementation Details. All training can be performed on a single GeForce RTX 4090 (See Appendix Fig. S1 and Fig. S2). We use the ADAM optimizer (Kingma & Ba, 2015) with an initial learning rate of 0.00025, which linearly decays over time. We report the hyperparameters of the architecture and training algorithm in Sec. A.2 (Tab. S1 and Tab. S2).

To examine emergent communication properties, we collect each agent's messages over all time steps in every episode. For the *ScoreG* task, messages are concatenated into a single message chain per agent per episode. In the *TemporalG* task, agents are only allowed to communicate when they occupy adjacent grid cells. Thus, we begin collecting messages only after their first adjacency and concatenate all subsequent messages. To decode environmental attributes, such as item scores, spawn times, and positions, from message chains, we use one-vs-rest logistic regression (LR). For example, to decode four possible item locations, we train four binary classifiers, each distinguishing one location from the rest. During inference, the class with the highest predicted probability is selected. Each LR model is trained on 3,500 message chains and tested on 1,500, using 3-fold cross-validation across 3 random seeds. We report message chain decoding accuracy as the average across all agents. Other metrics, including *LS*, *IC*, *topsim*, and *SR*, are computed using 1,000 test episodes.

5 Result

We investigate the emergence of linguistic properties in the FG framework according to previously stated research questions (**Q1-Q5**) and present our findings in this section. Each experimental setting is defined by four factors: the game type, agent population size, social structure, and training regime.

Table 1: **Cross-play training can cause non-interchangeable languages.** Game performance and language similarity (LS; Sec. A.3) comparison across different training regimes. N_{pop} is the population size. *Cross-SR* and *Self-SR* are the mean (± standard deviation) success rates when agents play with others or with copies of themselves, respectively.

Training	N_{pop}	LS	Cross-SR	Self-SR
XP	2	0.215 ± 0.002	0.987 ± 0.002	0.065 ± 0.054
XP+SP	2	0.598 ± 0.010	0.968 ± 0.005	0.968 ± 0.002
XP	3	0.527 ± 0.036	0.977 ± 0.007	0.944 ± 0.018

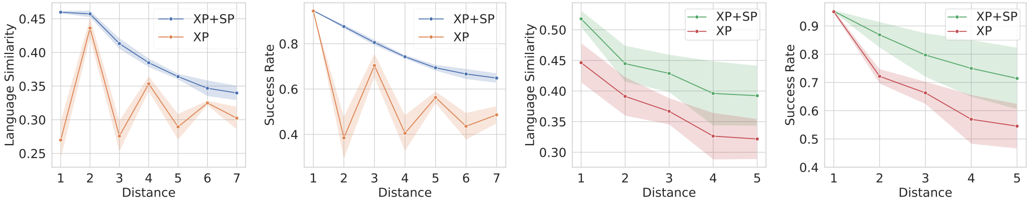

(a) *LS* (b) *SR* (c) *LS* (d) *SR*

Figure 3: **Self-Play (SP) promotes cultural transmission across social networks ($N_{\text{pop}} = 15$):** We plot *LS* and *SR* (see Sec. A.3) as a function of the shortest-path distance between two agents. (a,b) ring-structured network (Ring). (c,d) ring-structured with clique network (Clq).

These factors influence the emergence of different language properties, making exhaustive analysis infeasible. Instead, we report results from a representative subset of settings. For clarity, we adopt the naming convention for each experimental setting: `[game]-[population size]-[social structure]-[training regime]`. For example, *ScoreG*-P15-Ring-XP+SP refers to a setting where $N_{\text{pop}} = 15$ agents in a ring-structured network are trained with XP+SP regime on the *ScoreG* game. This convention is used throughout our analysis.

Increasing population size and self-play training support interchangeable language [*ScoreG*-FC]. Since decentralized agents do not share neural network parameters, it is natural to wonder whether they develop a common language at all. A curious possibility is that one agent might produce L1 while only understanding L2, with the other doing the opposite. Moreover, it is possible that an agent trained with its partner does not understand the language it produces. As shown in Tab. 1, XP agents trained exclusively with each other fail to understand their own messages when paired with a copy of themselves during test time as indicated by a drop of 6% in *Self-SR*. Surprisingly, when agents are trained with $N_{\text{pop}} = 3$, they maintain high *Self-SR* even without explicit self-play, suggesting that population training encourages the emergence of interchangeable language. These agents also develop more consistent language, as indicated by a higher *LS* of 0.53 compared to the XP alone. Furthermore, XP+SP agents achieve high *Self-SR* due to their direct exposure to SP. Interestingly, they also exhibit greater *LS* across agents, with an *LS* of 0.59, outperforming XP agents even in population settings. Agents with high *LS* produce similar messages, while agents with low *LS* produce distinct ones in the embedding space (Fig. S4). In agreement with prior research, (Dubova & Moskvichev, 2020) found that both population training with $N_{\text{pop}} \geq 3$ and the use of SP facilitate the development of common language.

Self-play enhances cultural transmission in weakly-connected networks [*ScoreG*-P15]. Human language evolves in sparsely connected societies, giving rise to a shared language alongside dialects and foreign languages. To investigate how language propagates in such settings, we train agents within weakly connected Ring and Clq social networks. The population size is fixed at $N_{\text{pop}} = 15$, with each agent interacting only with a few neighbors. This setup allows us to examine how culture is transmitted across indirect connections at test time. As shown in Fig. 3, both *LS* and *SR* generally decline with increasing distance between agents. This indicates that language partially propagates through non-co-trained agents: nearby neighbors develop more similar languages than distant ones. Importantly, the learned language also generalizes to indirectly connected agents, albeit with reduced *SR*. An exception arises for XP agents under the Ring network, which display a distinctive zig-zag pattern in Fig. 3a and Fig. 3b. Here, an agent produces messages more similar to those of a non-neighbor than to its direct partner (Fig. S5c). While agents successfully learn to interpret their neighbors, they fail to produce messages aligned with the language they understand (Fig. S5c and Fig. S6c), highlighting a breakdown in interchangeability. Furthermore, as shown

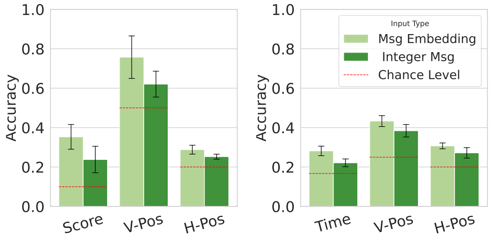

(a) *ScoreG* (b) *TemporalG*

Figure 4: **Decoding item states from messages.** *V-Pos*/*H-Pos* are item positions, *Score* is item value, and *Time* is item spawn time. *Integer Msg* uses raw message chains composed of integer sequences. *Msg Embedding* uses chained embeddings mapped from a lookup table. Error bars show standard deviations.

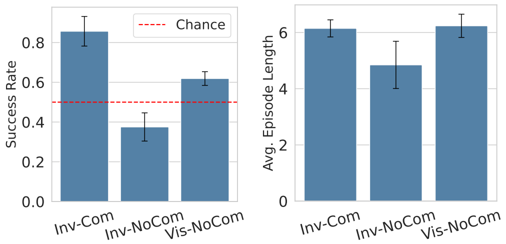

(a) Success Rate (b) Avg Ep Length

Figure 5: **Implicit communication in the *ScoreG* games.** *Inv*/*Vis* denote partner visibility; *Com*/*NoCom* indicate presence or absence of verbal communication. Item scores are from $[160, 162, \ldots, 240]$. We report average successful episode length; error bars show standard deviations across seeds and agents.

in Fig. 3a and Fig. 3c, self-play training yields consistently higher *LS* across all social distances compared to cross-play training. Together, these findings suggest that self-play not only enhances within-agent consistency but also supports more stable and transmissible communication protocols in structured populations. Finally, we find that adding more connections to Ring can greatly enhance cultural transmission (Fig. S7).

Spatial and temporal displacement emerge in agent communication [P3-FC-XP]. Humans can refer to past or future events, for example, I saw an apple yesterday or I will collect an apple tomorrow. They can also refer to spatially distant objects, such as an apple in the forest. This ability to refer to things beyond the immediate here and now is known as displacement in natural language. We investigate whether displacement can emerge in artificial foraging agents using the *TemporalG* game. XP agents with $N_{\text{pop}} = 3$ achieve strong performance in this setting, with a Cross-SR of 0.975 and a Self-SR of 0.962 (Tab. S11). Since the communication range is limited, the agents adopt a rendezvous strategy, meeting near the center of the grid map to establish communication (Fig. S11). Next, we decode spatial and temporal displacement information from the messages. The items can take on one of 6 possible spawn times, 4 vertical positions (excluding the grid's center), and 5 possible horizontal positions. The decoding accuracy for the spawn time and position of items is above chance (Fig. 4b), suggesting that messages function as temporal adverbials and spatial references. We also decode items' scores and positions from XP agents ($N_{\text{pop}} = 3$) in the *ScoreG* game (Fig. 4a). The items can take on one of 10 possible score ranges, 2 possible vertical positions (top and bottom), and 5 possible horizontal positions. The results align with those observed in the *TemporalG* game. Moreover, compared to *Integer Msg*, decoding with chains of message embeddings yields higher accuracy, suggesting that these embeddings encode more meaningful and linearly separable spatial and temporal features. Interestingly, when agents collect targets remotely without movement, their messages stop conveying spatial information (Fig. S8), highlighting the role of embodiment in shaping language.

Implicit communication can emerge when explicit message communication is disabled [*ScoreG*-P3-FC-XP]. We study whether agents can convey information through their sequence of actions in an episode when the explicit communication channel is disabled. We conduct an ablation on two variables: partner visibility and the presence of explicit verbal communication. When a partner is invisible, their location appears as an unoccupied cell in the observing agent's receptive field. We train XP agents in *Inv-NoCom* and *Vis-NoCom*, where agents either have or lack partner visibility, but no explicit message communication is allowed. If an agent observes an extreme score (e.g., 222 or 22), it can confidently infer whether the item is a goal or not. To isolate this confounding factor, we evaluate agents only under the condition that both partners observe high scores. As shown in Fig. 5, *Inv-Com* agents (XP agents trained in our default FG environments) achieve SR of 85%. Without communication, *Inv-NoCom* agents perform below chance (40%), likely because they fail to coordinate goal pickup without seeing each other. See more failure analysis in Sec. C.6. Interestingly, *Vis-NoCom* agents achieve an SR of 60%, outperforming *Inv-NoCom*. This indicates that both *Inv-Com* and *Vis-NoCom* agents can glean information from their partners—either via explicit messages or by observing partners' actions. We also evaluate the average length of successful test episodes. Both *Inv-Com* and *Vis-NoCom* agents take around 6 steps, while *Inv-NoCom* agents

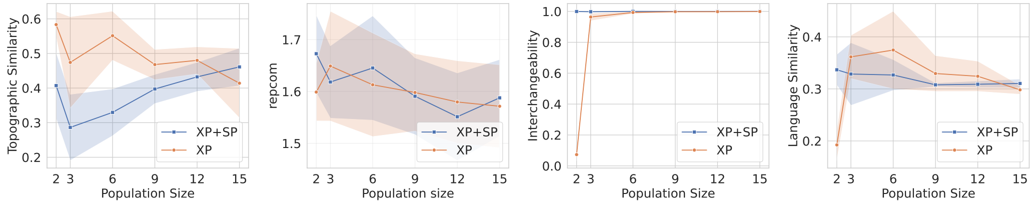

(a) *topsim* across N_{pop} (b) *repcom* across N_{pop} (c) *IC* across N_{pop} (d) *LS* across N_{pop}

Figure 6: **The effect of population training with fully-connected social networks on language properties.** (a) Topographic Similarity (*topsim*), (b) Representational Compositionality (*repcom*), (c) Interchangeability (*IC*), and (d) Language Similarity (*LS*) as a function of population sizes are shown. See Sec. A.3 for metrics details.

take about 5 steps. This indicates that agents with more accurate communication require extra steps to send meaningful signals, increasing their bandwidth and hence, longer episode length. Another possible strategy for implicit communication is bumping into each other; however, our analysis in Sec. C.7 shows this is not the case. The similar analysis above on implicit communication in *ScoreG* is also applicable in *TemporalG* (Sec. D.1). The result is consistent with prior research. Mordatch & Abbeel (2018) found that agents can use their physical body to send signals to others (e.g., through actions like pushing or pointing).

Population size affects language structure [*ScoreG*-FC]. Linguistic and cognitive studies suggest that larger communities are more likely to develop compositional languages (Reali et al., 2018; Raviv et al., 2019). Motivated by this, we examine how compositionality changes with population size. The results are shown in Fig. 6a. For *topsim*, XP agents exhibit a gradual decrease as population size increases, echoing prior findings in Rita et al. (2022). In contrast, XP+SP agents display a more stable upward trend in *topsim* with larger populations, suggesting that social training conditions help maintain or improve topographic structure even as group size grows. Turning to *repcom*, the new results reveal trends that differ from earlier observations. For XP agents, *repcom* now shows a slight but consistent downward trajectory as population size increases, with values slowly declining from size 2 to 15. XP+SP agents likewise exhibit a decreasing pattern. Taken together, these findings indicate that population size influences structural properties of the emergent language in distinct ways depending on the training setup. While *topsim* trends align with and extend previous studies reporting decreases (Rita et al., 2022) or stability (Michel et al., 2023), the updated *repcom* results suggest that larger populations do not necessarily enhance representational compositionality, offering a complementary perspective on how community size shapes emergent communication.

Population size affects language similarity and interchangeability [*ScoreG*-FC]. We observed that a population of three agents can develop a shared, interchangeable language. We now ask whether this effect persists as the population size increases. Fig. 6c shows that IC quickly saturates to nearly 1.0 for XP agents once the population size exceeds 2. This indicates that agents can understand their own messages. For XP+SP agents, IC reaches the maximum level across $N_{\text{pop}} \geq 2$. As shown in Fig. 6d, for XP agents, LS increases sharply from size 2 to 3, then gradually plateaus, indicating that training with multiple partners encourages the emergence of a shared protocol. XP+SP agents, in contrast, show consistently high LS across all population sizes. This suggests that self-play helps promote consistent, shared communication protocols within a population. Together, these results suggest that both self-play and population diversity contribute to the emergence of interchangeable and shared communication. Unlike our findings, prior work (Kim & Oh, 2021) reported that larger population sizes reduce language similarity, as listeners adapt to multiple speaker-specific languages. This discrepancy may stem from their unidirectional communication and centralized training, resulting in different optimal solutions.

6 Discussion

Understanding the origins of language is a long-standing interdisciplinary challenge spanning linguistics, psychology, neuroscience, and artificial intelligence. Emergent language offers a useful way to explore which ecological and cognitive factors could support the development of structured communication. In this work, we examine how communication emerges in multi-agent Foraging Games under different environmental and social pressures. Our simulations provide insight into when and why agents benefit from communicating in cooperative settings. In the non-cooperative control experiment (Sec. C.3), communication did not arise at all, indicating that cooperation is the pressure that makes signaling useful in this environment (Tomasello, 2010).

Importantly, the agents are not exposed to human language, yet under cooperative pressures and partial observability, they develop behaviors exhibiting several properties discussed in linguistic theory (Hockett, 1960). **Interchangeability** emerges through self-play training or social interactions within larger populations (Tab. 1). **Arbitrariness** is demonstrated by two cross-play agents developing non-interchangeable languages that are nonetheless mutually intelligible enough to enable successful cooperation and a high task success rate (Tab. 1 and Fig. S4a). **Compositionality** is indicated by high *repcom* and *topsim* scores (Fig. 6b, Fig. 6a). **Displacement** is demonstrated by above-chance linear decoding accuracy of items' positions, scores, and spawn times, showing that agents can refer to when and where currently invisible events happen (Fig. 4a). **Cultural transmission** is evidenced by the gradual decline in LS and SR with increasing distance in structured populations, despite no direct training between distant pairs (Fig. 3, Fig. S5d, Fig. S6d). This suggests that culture is transmitted and shaped through interaction within structured social networks. Our framework also shows that communication can emerge in both implicit and explicit forms, which standard referential games do not support.

We emphasize that these should be interpreted as functional analogues within the simulated environment, not as claims about human language evolution. Rather, they illustrate how certain communicative capacities can arise from ecological structure, shared intentions, and learning dynamics in multi-agent systems.

Despite these contributions, our work has several limitations. The language that emerges in FG is not directly comparable to natural language: it remains simple and lacks syntax, morphology, and other structural features of human communication. FG also provides limited semantic richness, as agents communicate primarily about a small set of task variables (time, location, and score). More broadly, emergent languages can show both similarities (Yao et al., 2022; Boldt & Mortensen, 2025) and clear divergences (Kottur et al., 2017; Chaabouni et al., 2019) from natural language, and it remains an open question whether they can be made substantially more human-like or interpretable.

Achieving this likely requires environments with richer, more open-ended semantics that naturally support broader, more compositional, and potentially syntactically structured communication. Such environments are not present in our work or most prior studies. The standard architectures and learning algorithms used here may also struggle in these settings, and progress will require advances in multi-agent learning and representation learning suited to more complex communicative demands. Moreover, our framework does not model interactional phenomena such as turn-taking, which pose additional challenges for current approaches.

Last but not least, the EC community still lacks a universal metric that captures the different forms of compositionality observed in emergent languages. The most commonly used measure, *topsim*, remains valuable for comparison across studies, but its theoretical relationship to compositionality is not fully established. The recently proposed *repcom* offers a stronger theoretical grounding in algorithmic information theory, yet relies on estimating Kolmogorov complexity, which depends on neural network model choices. Thus, different model architectures can yield different *repcom* scores. Developing metrics with both solid theoretical foundations and robust empirical behavior remains an open direction for future work.

References

Stefano V Albrecht and Subramanian Ramamoorthy. A game-theoretic model and best-response learning method for ad hoc coordination in multiagent systems. In *Proceedings of the 2013 international conference on Autonomous agents and multi-agent systems*, pp. 1155–1156, 2013.

Daniel S Bernstein, Robert Givan, Neil Immerman, and Shlomo Zilberstein. The complexity of decentralized control of markov decision processes. *Mathematics of operations research*, 27(4): 819–840, 2002.

Léonard Blier and Yann Ollivier. The description length of deep learning models. In *Advances in Neural Information Processing Systems*, volume 31, 2018.

Brendon Boldt and David R Mortensen. A review of the applications of deep learning-based emergent communication. *Transactions on Machine Learning Research*, 2024.

Brendon Boldt and David R Mortensen. Searching for the most human-like emergent language. In *Proceedings of the 2025 Conference on Empirical Methods in Natural Language Processing*, pp. 23300–23318, 2025.

Henry Brighton and Simon Kirby. Understanding linguistic evolution by visualizing the emergence of topographic mappings. *Artificial life*, 12(2):229–242, 2006.

Aydar Bulatov, Yury Kuratov, and Mikhail Burtsev. Recurrent memory transformer. In *Advances in Neural Information Processing Systems*, volume 35, pp. 11079–11091, 2022.

Aydar Bulatov, Yuri Kuratov, Yermek Kapushev, and Mikhail Burtsev. Beyond attention: Breaking the limits of transformer context length with recurrent memory. In *Proceedings of the AAAI Conference on Artificial Intelligence*, volume 38, pp. 17700–17708, 2024.

Kalesha Bullard, Franziska Meier, Douwe Kiela, Joelle Pineau, and Jakob Foerster. Exploring zero-shot emergent communication in embodied multi-agent populations. *arXiv preprint arXiv:2010.15896*, 2020.

Angelo Cangelosi. Evolution of communication and language using signals, symbols, and words. *IEEE Transactions on Evolutionary Computation*, 5(2):93–101, 2001.

Angelo Cangelosi and Domenico Parisi. The emergence of a'language'in an evolving population of neural networks. *Connection Science*, 10(2):83–97, 1998.

Angelo Cangelosi and Domenico Parisi. *Simulating the evolution of language*. Springer Science & Business Media, 2012.

Boaz Carmeli, Ron Meir, and Yonatan Belinkov. Ctd: Composition through decomposition in emergent communication. In *International Conference on Learning Representations*, 2025.

Rahma Chaabouni, Eugene Kharitonov, Emmanuel Dupoux, and Marco Baroni. Anti-efficient encoding in emergent communication. In *Advances in Neural Information Processing Systems*, volume 32, 2019.

Rahma Chaabouni, Eugene Kharitonov, Diane Bouchacourt, Emmanuel Dupoux, and Marco Baroni. Compositionality and generalization in emergent languages. In *Proceedings of the 58th Annual Meeting of the Association for Computational Linguistics*, pp. 4427–4442, 2020.

Rahma Chaabouni, Florian Strub, Florent Altché, Eugene Tarassov, Corentin Tallec, Elnaz Davoodi, Kory Wallace Mathewson, Olivier Tieleman, Angeliki Lazaridou, and Bilal Piot. Emergent communication at scale. In *International conference on learning representations*, 2022.

Rujikorn Charakorn, Poramate Manoonpong, and Nat Dilokthanakul. Generating diverse cooperative agents by learning incompatible policies. In *International Conference on Learning Representations*, 2023.

Rujikorn Charakorn, Poramate Manoonpong, and Nat Dilokthanakul. Diversity is not all you need: Training a robust cooperative agent needs specialist partners. In *Advances in Neural Information Processing Systems*, volume 37, pp. 56401–56423, 2024.

Morten H Christiansen and Simon Kirby. *Language evolution*. OUP Oxford, 2003.

Christian Schroeder De Witt, Tarun Gupta, Denys Makoviichuk, Viktor Makoviychuk, Philip HS Torr, Mingfei Sun, and Shimon Whiteson. Is independent learning all you need in the starcraft multi-agent challenge? *arXiv preprint arXiv:2011.09533*, 2020.

Kevin Yandoka Denamganai, Tim Bradley, Pierluigi Vito Amadori, Sondess Missaoui, Guy Moss, and James Alfred Walker. Erelela: Exploration in reinforcement learning via emergent language abstractions. 2024.

Jean-Louis Dessalles. *Why we talk: The evolutionary origins of language*. Oxford University Press, 2007.

Tabea Dreyer, Amir Haluts, Amos Korman, Nir Gov, Ehud Fonio, and Ofer Feinerman. Comparing cooperative geometric puzzle solving in ants versus humans. *Proceedings of the National Academy of Sciences*, 122(1):e2414274121, 2025.

Marina Dubova and Arseny Moskvichev. Effects of supervision, population size, and self-play on multi-agent reinforcement learning to communicate. In *Artificial Life Conference Proceedings 32*, pp. 678–686. MIT Press One Rogers Street, Cambridge, MA 02142-1209, USA journals-info . . . , 2020.

Marina Dubova, Arsenii Kirillovich Moskvichev, and Rob Goldstone. Reinforcement communication learning in different social network structures. In *Language in Reinforcement Learning Workshop at ICML*, 2020.

Eric Elmoznino, Thomas Jiralerspong, Yoshua Bengio, and Guillaume Lajoie. Towards a formal theory of representational compositionality. In *International Conference on Machine Learning*, 2025.

Katrina Evtimova, Andrew Drozdov, Douwe Kiela, and Kyunghyun Cho. Emergent communication in a multi-modal, multi-step referential game. In *International Conference on Learning Representations*, 2018.

Jakob Foerster, Ioannis Alexandros Assael, Nando De Freitas, and Shimon Whiteson. Learning to communicate with deep multi-agent reinforcement learning. In *Advances in Neural Information Processing Systems*, volume 29, 2016.

Lukas Galke, Yoav Ram, and Limor Raviv. Emergent communication for understanding human language evolution: What's missing? In *Emergent Communication Workshop at ICLR*, 2022.

Laura Harding Graesser, Kyunghyun Cho, and Douwe Kiela. Emergent linguistic phenomena in multi-agent communication games. In *Proceedings of the 2019 Conference on Empirical Methods in Natural Language Processing and the 9th International Joint Conference on Natural Language Processing (EMNLP-IJCNLP)*, pp. 3700–3710, 2019.

Niko A Grupen, Daniel D Lee, and Bart Selman. Multi-agent curricula and emergent implicit signaling. In *Proceedings of the 21st International Conference on Autonomous Agents and Multiagent Systems*, pp. 553–561, 2022.

Eleonora Gualdoni, Mycal Tucker, Roger Levy, and Noga Zaslavsky. Bridging semantics and pragmatics in information-theoretic emergent communication. In *Advances in Neural Information Processing Systems*, volume 37, pp. 21059–21078, 2024.

Irina Higgins, Loic Matthey, Arka Pal, Christopher Burgess, Xavier Glorot, Matthew Botvinick, Shakir Mohamed, and Alexander Lerchner. beta-vae: Learning basic visual concepts with a constrained variational framework. In *International conference on learning representations*, 2017.

Sepp Hochreiter and Jürgen Schmidhuber. Long short-term memory. *Neural computation*, 9(8): 1735–1780, 1997.

Charles F Hockett. The origin of speech. *Scientific American*, 203(3):88–97, 1960.

Shengyi Huang, Rousslan Fernand Julien Dossa, Chang Ye, Jeff Braga, Dipam Chakraborty, Kinal Mehta, and João GM Araújo. Cleanrl: High-quality single-file implementations of deep reinforcement learning algorithms. *Journal of Machine Learning Research*, 23(274):1–18, 2022.

K Ikram, E Mondragon, E Alonso, and M Garcia-Ortiz. Hexajungle: a marl simulator to study the emergence of language. In *Conference on Computer Vision and Pattern Recognition (CVPR 2021), Embodied AI Workshop*, pp. 20–25, 2021.

Taher Jafferjee, Juliusz Ziomek, Tianpei Yang, Zipeng Dai, Jianhong Wang, Matthew Taylor, Kun Shao, Jun Wang, and David Mguni. Taming multi-agent reinforcement learning with estimator variance reduction. *arXiv preprint arXiv:2209.01054*, 2022.

Unnat Jain, Luca Weihs, Eric Kolve, Mohammad Rastegari, Svetlana Lazebnik, Ali Farhadi, Alexander G Schwing, and Aniruddha Kembhavi. Two body problem: Collaborative visual task completion. In *Proceedings of the IEEE/CVF Conference on Computer Vision and Pattern Recognition*, pp. 6689–6699, 2019.

Natasha Jaques, Angeliki Lazaridou, Edward Hughes, Caglar Gulcehre, Pedro Ortega, DJ Strouse, Joel Z Leibo, and Nando De Freitas. Social influence as intrinsic motivation for multi-agent deep reinforcement learning. In *International conference on machine learning*, pp. 3040–3049. PMLR, 2019.

Ivana Kajic, Eser Aygün, and Doina Precup. Learning to cooperate: Emergent communication in multi-agent navigation. In *CogSci*, 2020.

Eugene Kharitonov, Rahma Chaabouni, Diane Bouchacourt, and Marco Baroni. Egg: a toolkit for research on emergence of language in games. In *Proceedings of the 2019 Conference on Empirical Methods in Natural Language Processing and the 9th International Joint Conference on Natural Language Processing (EMNLP-IJCNLP): System Demonstrations*, pp. 55–60, 2019.

Jooyeon Kim and Alice Oh. Emergent communication under varying sizes and connectivities. In *Advances in Neural Information Processing Systems*, volume 34, pp. 17579–17591, 2021.

Diederik P Kingma and Jimmy Ba. Adam: A method for stochastic optimization. In *International Conference on Learning Representations*, 2015.

Diederik P Kingma, Max Welling, et al. Auto-encoding variational bayes. In *International conference on learning representations*, 2014.

Simon Kirby, Mike Dowman, and Thomas L Griffiths. Innateness and culture in the evolution of language. *Proceedings of the National Academy of Sciences*, 104(12):5241–5245, 2007.

Simon Kirby, Tom Griffiths, and Kenny Smith. Iterated learning and the evolution of language. *Current opinion in neurobiology*, 28:108–114, 2014.

Satwik Kottur, José Moura, Stefan Lee, and Dhruv Batra. Natural language does not emerge 'naturally'in multi-agent dialog. In *Proceedings of the 2017 Conference on Empirical Methods in Natural Language Processing*, pp. 2962–2967, 2017.

Angeliki Lazaridou and Marco Baroni. Emergent multi-agent communication in the deep learning era. *arXiv preprint arXiv:2006.02419*, 2020.

Angeliki Lazaridou, Alexander Peysakhovich, and Marco Baroni. Multi-agent cooperation and the emergence of (natural) language. In *International Conference on Learning Representations*, 2017.

Angeliki Lazaridou, Karl Moritz Hermann, Karl Tuyls, and Stephen Clark. Emergence of linguistic communication from referential games with symbolic and pixel input. In *International Conference on Learning Representations*, 2018.

David Lewis. *Convention: A philosophical study*. John Wiley & Sons, 2008.

Chuming Li, Jie Liu, Yinmin Zhang, Yuhong Wei, Yazhe Niu, Yaodong Yang, Yu Liu, and Wanli Ouyang. Ace: Cooperative multi-agent q-learning with bidirectional action-dependency. In *Proceedings of the AAAI conference on artificial intelligence*, volume 37, pp. 8536–8544, 2023.

Dapeng Li, Zhiwei Xu, Bin Zhang, Guangchong Zhou, Zeren Zhang, and Guoliang Fan. From explicit communication to tacit cooperation: A novel paradigm for cooperative marl. In *Proceedings of the 23rd International Conference on Autonomous Agents and Multiagent Systems*, pp. 2360–2362, 2024.

Sheng Li, Jayesh K Gupta, Peter Morales, Ross Allen, and Mykel J Kochenderfer. Deep implicit coordination graphs for multi-agent reinforcement learning. In *Proceedings of the 20th International Conference on Autonomous Agents and MultiAgent Systems*, pp. 764–772, 2021.

Olaf Lipinski, Adam J Sobey, Federico Cerutti, and Timothy J Norman. It's about time: Temporal references in emergent communication. *arXiv preprint arXiv:2310.06555*, 2023.

Olaf Lipinski, Adam Sobey, Federico Cerutti, and Timothy Norman. Speaking your language: Spatial relationships in interpretable emergent communication. In *Advances in Neural Information Processing Systems*, volume 37, pp. 140113–140137, 2024.

Bo Liu, Leon Guertler, Simon Yu, Zichen Liu, Penghui Qi, Daniel Balcells, Mickel Liu, Cheston Tan, Weiyan Shi, Min Lin, et al. Spiral: Self-play on zero-sum games incentivizes reasoning via multi-agent multi-turn reinforcement learning. *arXiv preprint arXiv:2506.24119*, 2025a.

Yuxi Liu, Konpat Preechakul, Kananart Kuwaranancharoen, and Yutong Bai. The serial scaling hypothesis. *arXiv preprint arXiv:2507.12549*, 2025b.

Ryan Lowe, Abhinav Gupta, Jakob Foerster, Douwe Kiela, and Joelle Pineau. On the interaction between supervision and self-play in emergent communication. In *International Conference on Learning Representations*, 2020.

Paul Michel, Mathieu Rita, Kory Wallace Mathewson, Olivier Tieleman, and Angeliki Lazaridou. Revisiting populations in multi-agent communication. In *International Conference on Learning Representations*, 2023.

Volodymyr Mnih, Koray Kavukcuoglu, David Silver, Alex Graves, Ioannis Antonoglou, Daan Wierstra, and Martin Riedmiller. Playing atari with deep reinforcement learning. *arXiv preprint arXiv:1312.5602*, 2013.

Volodymyr Mnih, Koray Kavukcuoglu, David Silver, Andrei A Rusu, Joel Veness, Marc G Bellemare, Alex Graves, Martin Riedmiller, Andreas K Fidjeland, Georg Ostrovski, et al. Human-level control through deep reinforcement learning. *nature*, 518(7540):529–533, 2015.

Igor Mordatch and Pieter Abbeel. Emergence of grounded compositional language in multi-agent populations. In *Proceedings of the AAAI conference on artificial intelligence*, volume 32, 2018.

Jesse Mu and Noah Goodman. Emergent communication of generalizations. In *Advances in Neural Information Processing Systems*, volume 34, pp. 17994–18007, 2021.

Yao Mu, Shunyu Yao, Mingyu Ding, Ping Luo, and Chuang Gan. Ec2: Emergent communication for embodied control. In *Proceedings of the IEEE/CVF Conference on Computer Vision and Pattern Recognition*, pp. 6704–6714, 2023.

Mitja Nikolaus. Emergent communication with conversational repair. In *International Conference on Learning Representations*, 2024.

Martin A Nowak and Natalia L Komarova. Towards an evolutionary theory of language. *Trends in cognitive sciences*, 5(7):288–295, 2001.

Martin A Nowak, Joshua B Plotkin, and Vincent AA Jansen. The evolution of syntactic communication. *Nature*, 404(6777):495–498, 2000.

Georgios Papoudakis, Filippos Christianos, and Stefano Albrecht. Agent modelling under partial observability for deep reinforcement learning. In *Advances in Neural Information Processing Systems*, volume 34, pp. 19210–19222, 2021.

Shivansh Patel, Saim Wani, Unnat Jain, Alexander G Schwing, Svetlana Lazebnik, Manolis Savva, and Angel X Chang. Interpretation of emergent communication in heterogeneous collaborative embodied agents. In *Proceedings of the IEEE/CVF International Conference on Computer Vision*, pp. 15953–15963, 2021.

Jannik Peters, Constantin Waubert de Puiseau, Hasan Tercan, Arya Gopikrishnan, Gustavo Adolpho Lucas de Carvalho, Christian Bitter, and Tobias Meisen. Emergent language: a survey and taxonomy. *Autonomous Agents and Multi-Agent Systems*, 39(1):1–73, 2025.

Limor Raviv, Antje Meyer, and Shiri Lev-Ari. Larger communities create more systematic languages. *Proceedings of the Royal Society B*, 286(1907):20191262, 2019.

Florencia Reali, Nick Chater, and Morten H Christiansen. Simpler grammar, larger vocabulary: How population size affects language. *Proceedings of the Royal Society B: Biological Sciences*, 285 (1871):20172586, 2018.

Mathieu Rita, Florian Strub, Jean-Bastien Grill, Olivier Pietquin, and Emmanuel Dupoux. On the role of population heterogeneity in emergent communication. In *International Conference on Learning Representations*, 2022.

Mikayel Samvelyan, Akbir Khan, Michael D Dennis, Minqi Jiang, Jack Parker-Holder, Jakob Nicolaus Foerster, Roberta Raileanu, and Tim Rocktäschel. Maestro: Open-ended environment design for multi-agent reinforcement learning. In *International Conference on Learning Representations*, 2023.

John Schulman, Philipp Moritz, Sergey Levine, Michael Jordan, and Pieter Abbeel. High-dimensional continuous control using generalized advantage estimation. In *International Conference on Learning Representations*, 2016.

John Schulman, Filip Wolski, Prafulla Dhariwal, Alec Radford, and Oleg Klimov. Proximal policy optimization algorithms. *arXiv preprint arXiv:1707.06347*, 2017.

Kim Sterelny. Language, gesture, skill: the co-evolutionary foundations of language. *Philosophical Transactions of the Royal Society B: Biological Sciences*, 367(1599):2141–2151, 2012.

Mingfei Sun, Sam Devlin, Jacob Beck, Katja Hofmann, and Shimon Whiteson. Trust region bounds for decentralized ppo under non-stationarity. In *Proceedings of the 2023 International Conference on Autonomous Agents and Multiagent Systems*, pp. 5–13, 2023.

Valentin Taillandier, Dieuwke Hupkes, Benoît Sagot, Emmanuel Dupoux, and Paul Michel. Neural agents struggle to take turns in bidirectional emergent communication. In *International Conference on Learning Representations*, 2023.

Michael Tomasello. *Origins of human communication*. MIT press, 2010.

Ryo Ueda and Tadahiro Taniguchi. Lewis's signaling game as beta-vae for natural word lengths and segments. In *International Conference on Learning Representations*, 2024.

Kyle Wagner, James A Reggia, Juan Uriagereka, and Gerald S Wilkinson. Progress in the simulation of emergent communication and language. *Adaptive Behavior*, 11(1):37–69, 2003.

Han Wang, Binbin Chen, Tieying Zhang, and Baoxiang Wang. Learning to communicate through implicit communication channels. In *International Conference on Learning Representations*, 2025a.

Kevin Wang, Ishaan Javali, MichaĹ Bortkiewicz, Benjamin Eysenbach, et al. 1000 layer networks for self-supervised rl: Scaling depth can enable new goal-reaching capabilities. In *Advances in Neural Information Processing Systems*, 2025b.

Erik Wijmans, Abhishek Kadian, Ari Morcos, Stefan Lee, Irfan Essa, Devi Parikh, Manolis Savva, and Dhruv Batra. Dd-ppo: Learning near-perfect pointgoal navigators from 2.5 billion frames. In *International Conference on Learning Representations*, 2020.

Ludwig Wittgenstein. *Philosophical investigations*. John Wiley & Sons, 2009.

Yaodong Yang, Guangyong Chen, Weixun Wang, Xiaotian Hao, Jianye Hao, and Pheng-Ann Heng. Transformer-based working memory for multiagent reinforcement learning with action parsing. In *Advances in Neural Information Processing Systems*, volume 35, pp. 34874–34886, 2022.

Shunyu Yao, Mo Yu, Yang Zhang, Karthik Narasimhan, Joshua Tenenbaum, and Chuang Gan. Linking emergent and natural languages via corpus transfer. In *International Conference on Learning Representations*, 2022.

Chao Yu, Akash Velu, Eugene Vinitsky, Jiaxuan Gao, Yu Wang, Alexandre Bayen, and Yi Wu. The surprising effectiveness of ppo in cooperative multi-agent games. In *Advances in Neural Information Processing Systems*, volume 35, pp. 24611–24624, 2022.

Rotem Zion, Boaz Carmeli, Orr Paradise, and Yonatan Belinkov. Semantics and spatiality of emergent communication. In *Advances in Neural Information Processing Systems*, volume 37, pp. 110156–110196, 2024.

A Implementation and Training Details

A.1 Learning to Communicate with PPO

Agents in our setting learn to act and communicate simultaneously. As illustrated in Fig. 2, each agent receives an observation from the environment and a message from its partner sent at the previous time step. Based on this input, the agent produces a discrete action and message. During training, the agent also estimates a value function to guide learning. In the following, we formalize this process using the multi-agent reinforcement learning (MARL) framework and describe how action and communication are jointly optimized via the MARL algorithm. The method most closely related to ours is RIAL (Foerster et al., 2016). However, unlike RIAL and related approaches, we do not assume parameter sharing or use a centralized critic. While Independent PPO (De Witt et al., 2020) employs parameter sharing among independent agents, a technique that can help stabilize learning (Sun et al., 2023), our method explicitly removes this parameter sharing. These design choices make our setting more reflective of human-like conditions, where individuals operate independently and learn through decentralized interaction. Moreover, by avoiding parameter sharing, our method enables the study of linguistic and behavioral heterogeneity across agents.

Problem Formulation Our learning setting is a two-player variant of decentralized partially observable Markov decision processes (DecPOMDP) (Bernstein et al., 2002). A two-player DecPOMDP with communication is formally defined as the tuple $(S, \mathcal{A}_1, \mathcal{A}_2, \mathcal{M}_1, \mathcal{M}_2, \Omega_1, \Omega_2, T, O, r, \gamma, H)$, where S represents the state space, $\mathcal{A} \equiv \mathcal{A}_1 \times \mathcal{A}_2$ denotes the joint-action space, $\mathcal{M} \equiv \mathcal{M}_1 \times \mathcal{M}_2$ denotes the joint-message space, $\Omega \equiv \Omega_1 \times \Omega_2$ signifies the joint-observation space (where Ω_1 and Ω_2 are the individual observation spaces), $T(s'|s, a_1, a_2)$ provides the transition probability from state s to s' upon executing the joint action (a_1, a_2), $O(o_1, o_2|s)$ represents the conditional probability of observing the joint observation (o_1, o_2) given the current state s, $r(s, a_1, a_2)$ is the shared reward function, γ is the discount factor for rewards, and H denotes the horizon length.

The first and second agents are controlled by neural policies $\psi_1 = (\pi_1, \phi_1)$ and $\psi_2 = (\pi_2, \phi_2)$, respectively, where the subscript indicates the agent identity. Here, π denotes the action policy and ϕ denotes the communication policy. Each neural policy ψ is parameterized by θ. At each time step t, agents receive the joint observation $o^{(t)} = (o_1^{(t)}, o_2^{(t)})$ and the previous joint message $m^{(t-1)} = (m_1^{(t-1)}, m_2^{(t-1)})$. Each agent i maintains a trajectory $\tau_i^{(t)}$ consisting of its own history up to time t. Conditioned on its trajectory $\tau_i^{(t)}$ and the other agent's previous message $m_j^{(t-1)}$, agent i samples its action and message as follows: $a_i^{(t)} \sim \pi_i(a_i^{(t)} \mid m_j^{(t-1)}, \tau_i^{(t)})$ and $m_i^{(t)} \sim \phi_i(m_i^{(t)} \mid m_j^{(t-1)}, \tau_i^{(t)})$. The joint trajectory can be written as $\tau = (o_0, a_0, m_0, r_1, o_1, ..., o_{H-1}, a_{H-1}, m_{H-1}, r_H, o_H) \in \mathcal{T} \equiv (\Omega \times \mathcal{A} \times \mathcal{M} \times \mathbb{R})^H$. The return of a trajectory τ is defined as $G(\tau) = \sum_{t=1}^{H} \gamma^{t-1} r_t$, and the expected return of the joint policy (ψ_1, ψ_2) is $J(\psi_1, \psi_2) = \mathbb{E}_{\tau \sim p(\tau|\theta_1, \theta_2)} G(\tau)$, where $p(\tau|\theta_1, \theta_2)$ denotes the distribution over trajectories induced by the joint policy.

Learning to Act and Communicate with PPO As described above, we treat the communication policy the same as the action policy, i.e., we jointly optimize them with policy gradients. This is because both policies output discrete decisions based on the agent's observation history, and both can be optimized with similar objective functions under policy gradient methods. We use PPO (Schulman et al., 2017) because of its effectiveness in optimizing discrete actions, sample efficiency, and good performance in multi-agent learning (Li et al., 2023; De Witt et al., 2020; Yu et al., 2022). We first define $r_a^{(t)}(\theta) = \frac{\pi(a^{(t)}|\tau^{(t)})}{\pi_{\text{old}}(a^{(t)}|\tau^{(t)})}$ and $r_m^{(t)}(\theta) = \frac{\phi(m^{(t)}|\tau^{(t)})}{\phi_{\text{old}}(m^{(t)}|\tau^{(t)})}$ as the ratios of action policy and communication policy (Schulman et al., 2017), respectively. The objective function of the neural policy θ can be written as $\mathcal{J} = \mathcal{J}_a + \mathcal{J}_m + \mathcal{J}_{\text{ent}}$. We use Generalized Advantage Estimation (GAE) (Schulman et al., 2016) to estimate the advantage function. We use a single advantage function $\hat{A}^{(t)}$ estimated from the shared representation output by the LSTM, which is used for optimizing both the action and communication policies. Each agent is trained independently using standard single-agent PPO, which treats its partner as part of the environment, i.e., fully decentralized training. The first term optimizes the action policy π using the estimated advantage function:

$$\mathcal{J}_a = \mathbb{E}_{t,\tau \sim p(\tau|\theta,\cdot)} \left[\min \left(r_a^{(t)}(\theta) \hat{A}^{(t)},\ \text{clip}(r_a^{(t)}(\theta), 1-\epsilon, 1+\epsilon) \hat{A}^{(t)} \right) \right]. \tag{1}$$

The second term optimizes the communication policy ϕ in the same manner:

$$\mathcal{J}_m = \mathbb{E}_{t,\tau\sim p(\tau|\theta,\cdot)}\left[\min\left(r_m^{(t)}(\theta)\hat{A}^{(t)},\ \text{clip}(r_m^{(t)}(\theta),1-\epsilon,1+\epsilon)\hat{A}^{(t)}\right)\right]. \tag{2}$$

The final term encourages exploration by maximizing the entropy of both action and message distributions:

$$\mathcal{J}_{\text{ent}} = -\mathbb{E}_{t,\tau\sim p(\tau|\theta,\cdot)}\left[\lambda_a\sum_a \pi(a|\tau^{(t)})\log\pi(a|\tau^{(t)}) + \lambda_m\sum_m \phi(m|\tau^{(t)})\log\phi(m|\tau^{(t)})\right]. \tag{3}$$

Neural Architecture In Fig. 2, the agent architecture is divided into input and output components. The encoders are essential for converting heterogeneous inputs such as messages, grid observations, and spatial coordinates into a unified feature representation, enabling effective downstream processing and integration by the LSTM. On the input side, the *message encoder* $\mathcal{E}_{\mathcal{M}}$, *grid encoder* $\mathcal{E}_{\mathcal{X}}$, and *position encoder* $\mathcal{E}_{\mathcal{P}}$ process the incoming message from the other agent, the grid observation, and the agent's current position, respectively. The extracted features from these encoders are concatenated and fed into an LSTM (Hochreiter & Schmidhuber, 1997), which maintains temporal memory. On the output side, the *message head* $\mathcal{D}_{\mathcal{M}}$, *action head* $\mathcal{D}_{\mathcal{A}}$, and *value head* $\mathcal{D}_{\mathcal{V}}$ generate the outgoing message, the selected action, and the estimated state value, respectively. All encoders and heads are implemented as shallow multilayer perceptrons (MLPs). The message encoder $\mathcal{E}_{\mathcal{M}}$ includes an embedding layer that maps each vocabulary index to a real-valued vector before passing it to the MLP. Our code is built on the widely used PPO-LSTM implementation by Huang et al. (2022).

A.2 Model Training

We train our models on a single GeForce RTX 4090. However, due to the small model size and low environment complexity, training can also be run entirely on a CPU as well. For populations smaller than 3, training takes approximately 16 hours, depending on the CPU and the number of available cores. The longest training time occurs with a population size of 15 and takes up to 3 days. All experiments are repeated with three different random seeds. We use the ADAM optimizer (Kingma & Ba, 2015) with an initial learning rate of 0.00025, which linearly decays over time. We report the hyperparameters of the architecture and training algorithm in Tab. S1 and Tab. S2. The examples of learning dynamics for *ScoreG* and *TemporalG* are shown in Fig. S1 and Fig. S2.

Table S1: Neural architecture hyperparameters.

Component	**Hyperparameter**
Visual encoder	4-layer MLP: [256, 256, 128, 16]
Visual input shape	$(1, 5, 5)$ grayscale grid
Position encoder	Linear(2, 4)
Message embedding size	16
Message encoder	Embedding(Vocab. Size, 16) + Linear(16, 16)
LSTM hidden size	128
LSTM input size	16 (visual) $+$ 4 (position) $+$ 16 (message) = 36
Action head	Linear(128, `num_actions`)
Value head	Linear(128, 1)
Message head	Linear(128, 16)
Weight initialization	Orthogonal (std = $\sqrt{2}$), output layers: std = 0.01

A.3 Metrics

Topographic Similarity (topsim) Topographic similarity measures the alignment between the structure of the message space and the semantic space (e.g., environmental states or properties). It is defined as the Spearman rank correlation between all pairwise distances in these two spaces (Brighton & Kirby, 2006; Lazaridou et al., 2018). A higher *topsim* indicates a more compositional and consistent mapping between semantic meanings and messages. We define the semantic space using ground-truth attributes of the environment, specifically the scores and positions of items in the

Table S2: PPO hyperparameters.

Hyperparameter	**Value**
Total time steps	2×10^9
Learning rate	2.5×10^{-4}
Number of environments	128
Number of steps per rollout	32
Number of minibatches	4
Number of update epochs	4
Discount factor γ	0.99
GAE λ	0.95
Clip coefficient	0.1
Clip value loss	True
Normalize advantages	True
Action entropy coefficient	0.01
Message entropy coefficient	0.002
Value function coefficient	0.5
Max gradient norm	0.5
Learning rate annealing	True
Target KL divergence	None
Batch size	4096
Minibatch size	1024
Optimizer	Adam ($\epsilon = 10^{-5}$)

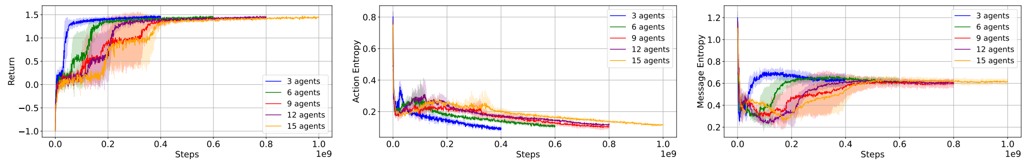

(a) Episodic return

(b) Action entropy

(c) Message entropy

Figure S1: **Larger population takes longer time to converge.** The figure shows learning dynamics of agents with different population sizes in *ScoreG*. Return, action entropy, and message entropy are plotted over environment steps, averaged across three seeds. A single step is defined as a single interaction with the environment.

ScoreG. To implement the topographic similarity metric, we use the EGG toolkit (Kharitonov et al., 2019).

Let $M = \{m_1, m_2, \ldots, m_N\}$ be the set of message sequences, and $S = \{s_1, s_2, \ldots, s_N\}$ be the corresponding semantic meanings. Let $\delta_M(m_i, m_j)$ and $\delta_S(s_i, s_j)$ denote the pairwise distance functions in the message and semantic spaces, respectively. Then:

$$\text{topsim} = \text{Spearman}\left(\{\delta_M(m_i, m_j)\}_{i<j}, \{\delta_S(s_i, s_j)\}_{i<j}\right) \tag{4}$$

A high topographic similarity indicates that similar messages correspond to similar semantic meanings, reflecting a structured and grounded communication protocol. We use items' positions and scores as semantic meanings.

Calculate Semantic Meaning Vectors: The semantic space is constructed from each item's spatial position and score. We represent the semantic state of item i as

$$S_i = [x_i,\, y_i,\, s_i],$$

where (x_i, y_i) denotes the item's location and s_i denotes its score. These semantic vectors are used to compute pairwise distances, which are then compared with pairwise message distances when calculating *topsim*.

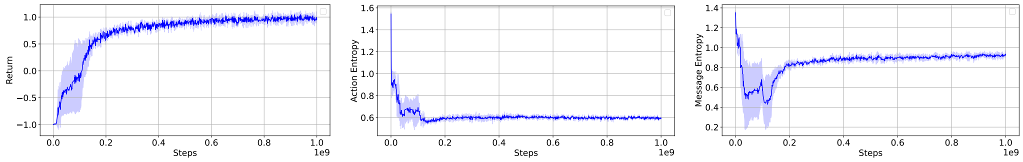

(a) Episodic return (b) Action entropy (c) Message entropy

Figure S2: **Learning dynamics of three XP agents in *TemporalG*.** Agents start to converge at around one billion environment steps.

Representational Compositionality (repcom) quantifies how well semantic representations can be reconstructed from messages using a low-complexity mapping function (Elmoznino et al., 2025). The metric is grounded in algorithmic information theory and is defined as a compression ratio that captures both the expressivity of the semantic space and the simplicity of the mapping from messages to meanings.

Let $S \in \mathbb{R}^{N \times D}$ be the matrix of semantic representations (one vector s_i per item), and let $M = \{m_1, m_2, \ldots, m_N\}$ be the corresponding discrete message sequences produced by the agents.

In the theoretical formulation, representational compositionality is defined as:

$$\text{repcom} = \frac{K(S)}{K(f) + K(S \mid M, f)}, \tag{5}$$

where f denotes the semantics function mapping messages to predicted semantic vectors, $K(f)$ is the Kolmogorov complexity of this mapping (its description length), and $K(S \mid M, f)$ is the number of bits required to encode S given that they are generated from messages via f. A language achieves high *repcom* when a *simple* mapping function f (low $K(f)$) can *accurately* reconstruct semantic vectors (low $K(S \mid M, f)$), indicating a systematic and compositional relationship between messages and meanings.

Since Kolmogorov complexities are not computable, we follow the empirical estimation procedure of Elmoznino et al. (2025), in which $K(S \mid M, f)$ is approximated using the model's prediction loss on semantic vectors. Given a parametric predictor f_θ trained to map each message m_i to its semantic meaning s_i, we estimate:

$$\widehat{K(S \mid M)} \;\approx\; \sum_{i=1}^{N} \mathcal{L}\big(s_i, f_\theta(m_i)\big), \tag{6}$$

where $\mathcal{L}$ is a reconstruction loss (e.g., mean squared error). Similarly, the complexity of the mapping $K(f)$ is approximated implicitly through the inductive bias and capacity of the predictor f_θ; simpler models correspond to lower effective complexity. In practice, $\mathcal{L}$ is calculated using prequential coding (Blier & Ollivier, 2018).

A higher *repcom* indicates that semantic representations can be generated from messages through a low-complexity, high-accuracy mapping, reflecting a structured and compositional communication protocol. In contrast, if reconstructing S requires a complex or arbitrary mapping, or if reconstruction is inaccurate, *repcom* decreases.

Language Similarity (LS) quantifies the token-level similarity between two agents based on their communication over multiple episodes, starting from the same initial condition. A higher score means the agents tend to use the same messages in similar contexts, indicating stronger convergence in their communication strategies. For a given episode e, the agents i and j produce their respective message sequences $M_i^{(e)}$ and $M_j^{(e)}$. Let $\mathcal{D}_{\text{edit}}(\cdot)$ represent the normalized edit distance function, and let N_e denote the total number of evaluation episodes. The Language Similarity (LS) between agents i and j is defined as:

$$\text{LS(i,j)} = \frac{1}{N_e} \sum_{e=1}^{N_e} 1 - \mathcal{D}_{\text{edit}}(M_i^{(e)}, M_j^{(e)}) \tag{7}$$

We can then compute the average LS across all pairs of agents in the entire population as follows: $\text{LS} = \frac{1}{N_{\text{pop}}(N_{\text{pop}}-1)} \sum_{i=1}^{N_{\text{pop}}} \sum_{j \neq i}^{N_{\text{pop}}} \text{LS}(i, j)$.

Interchangeability (IC) refers to a property of language wherein a speaker can both send and understand the same linguistic signals (Hockett, 1960). In the context of agents, this means that an agent should understand the language it produces. To evaluate interchangeability in agents, we embed the same neural network in two different agent bodies and assess their performance in the game. We compare an agent's success when paired with itself to its success when paired with other agents. Formally, consider a set of N_{pop} agents. Let $\text{SR}(i, j)$ denote the success rate of an agent i when playing with an agent j. Therefore, we propose that interchangeability (IC) can be defined as:

$$\text{IC} = (N_{\text{pop}} - 1) \times \frac{\sum_{i=1}^{N_{\text{pop}}} \text{SR}(i, i)}{\sum_{i=1}^{N_{\text{pop}}} \sum_{j \neq i}^{N_{\text{pop}}} \text{SR}(i, j)} \tag{8}$$

B Additional Experiments and Results on Cultural Transmission

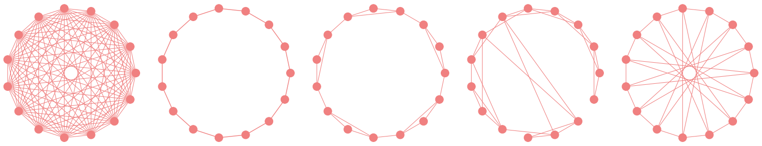

(a) FC (b) Ring (c) Clq (d) WS (e) LRC

Figure S3: **Social network structures:** Nodes represent agents, and edges denote pairs of agents that are co-trained. Network structures are abbreviated as follows: **FC – Fully Connected**, **Ring – Ring Structure**, **Clq – Ring with Cliques**, **WS – Watts-Strogatz**, and **LRC – Ring with Long-Range Connections**

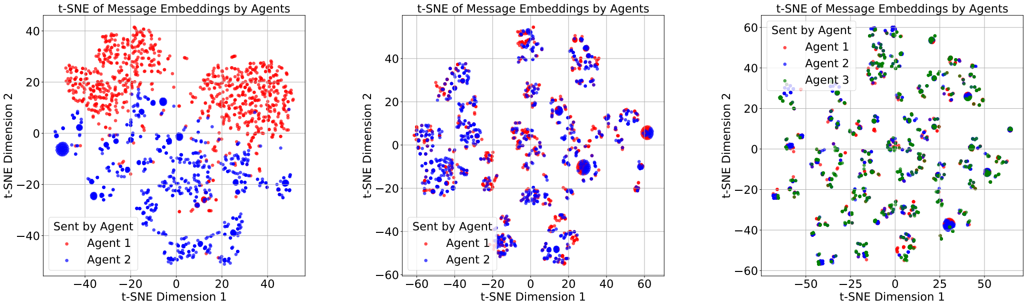

(a) 2 XP Agents (b) 2 XP+SP Agents (c) 3 XP Agents

Figure S4: **Message embeddings under different training regimes.** In the t-SNE space of embedding vectors, sequences of messages from two agents are clearly separable in the 2-XP-Agents setting. (a) Messages from different agents occupy distinct regions of the embedding space (indicating different languages). (b-c) Messages from different agents largely overlap (indicating similar languages).

We further examine whether adding additional connections, while keeping social networks sparse, can enhance cultural transmission. To this end, we employ two networks with small-world properties, as illustrated in Fig. S3. The first is the Watts-Strogatz (WS) network, constructed with parameters $k = 4$ (neighbors) and $\beta = 0.2$. The second is a ring structure with long-range connections (LRC) network, built upon a standard ring lattice with additional long-range edges. Specifically, the LRC network is generated by iteratively linking the farthest nodes on the ring lattice, serving as a simple proxy for reducing average path length and thereby producing a more small-world-like structure.

More cliques and long-range connections both enhance cultural transmission [ScoreG-P15-XP] We examine the impact of adding cliques or long-range connections to the ring-structured network

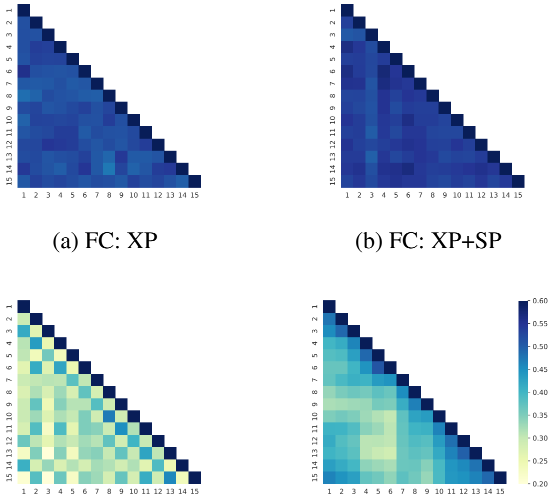

(a) FC: XP

(b) FC: XP+SP

(c) Ring: XP

(d) Ring: XP+SP

Figure S5: **Language Similarity (LS) between agent pairs under different social structures and training strategies.** (a–b) Under the fully connected (FC) social network, both training regimes (XP and XP+SP) yield similar languages across agents. (c) With XP training in the Ring network, agents develop different languages from their partners (evident from the color switching between light and dark along the axis perpendicular to the diagonal). (d) With XP+SP training in the Ring network, agents and their partners converge to similar languages.

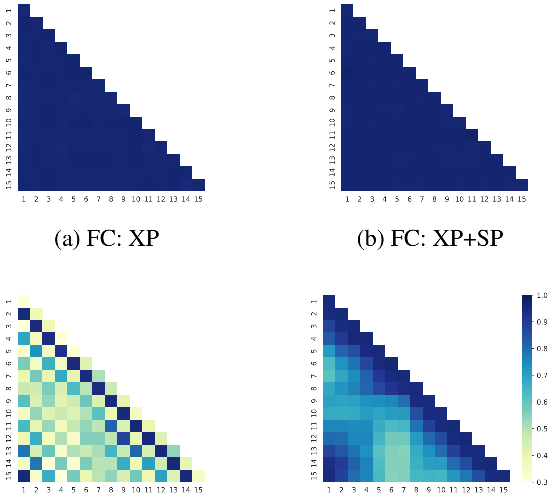

(a) FC: XP

(b) FC: XP+SP

(c) Ring: XP

(d) Ring: XP+SP

Figure S6: **Success Rates (SR) between agent pairs under different social structures and training strategies.** (a–b) Both XP and XP+SP produce homogeneous SR across all pairs. (c) With XP training in the Ring network, agents fail when paired with copies of themselves. (d) With XP+SP training in the Ring network, agents succeed when paired with themselves.

on language transmission. Results are shown in Fig. S7a and Fig. S7b. For WS and LRC, both LS and SR decrease slightly with social distance, demonstrating successful language transmission to non-co-trained agents in the population. For Clq, LS at distance 1 is already lower and declines more steeply with distance than the others. SR also falls sharply, dropping from 0.95 at distance 1 to 0.55 at distance 5. This result is intuitive because Clq is constructed by adding only five connections to the

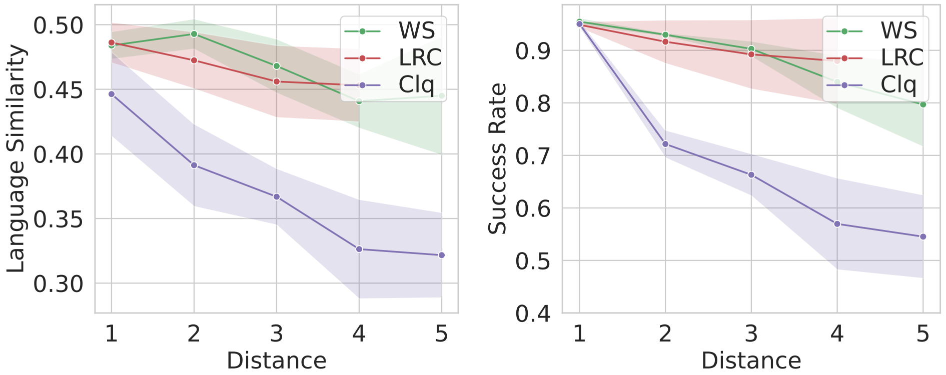

(a) *LS*

(b) *SR*

Figure S7: **More cliques and long-range connections both enhance cultural transmission** ($N_{\textbf{pop}} = 15$)**:** We plot *LS* and *SR* (See Sec. A.3) as a function of the shortest-path distance between two agents. A distance of 1 indicates that two agents were co-trained, while a distance greater than 1 indicates that the agents were never paired during training. Note that the maximum shortest path of LRC is only 4 while other cases are 5.

ring network, which may not be enough for the population to form similar and compatible languages, whereas the others are constructed by adding many more connections to the ring network.

C ScoreG: Additional Results and Analyses

C.1 Ablation: Disembodiment (Referential Game)

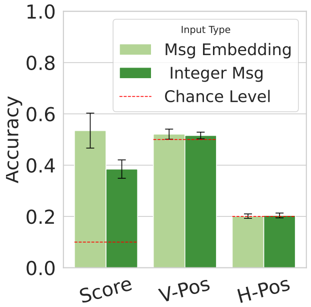

Figure S8: **Decoding item states from messages produced in a no-body referential game.** *V-Pos*/*H-Pos* are item positions, and *Score* is item value. *Integer Msg* uses raw message chains composed of integer sequences. *Msg Embedding* uses chained embeddings mapped from a lookup table. Error bars show standard deviations.

In this variant, agents are immobilized and remain fixed near their respective items. The game structure and goal are the same as those in *ScoreG*, but without requiring agents to move to pick up the target item. Specifically, the action space is restricted to {*select my item*, *select another item*, *idle*}. The game succeeds only if both agents correctly select the target item at the final timestep ($t = 6$). Any premature selection causes immediate failure. Rewards are binary: $+1$ for success and -1 for failure, with no advantage for finishing early since the episode length is fixed.

As shown in Fig. S8, agents exchange messages conveying *item score* information, but not spatial information, a result confirmed by chance-level decoding accuracy. Each agent still observes its own static position, which in principle allows item locations to be inferred. However, this positional information is task-irrelevant, as agents cannot move.

C.2 Ablation: Unidirectional Communication

We study a setting where only one agent (the sender) can transmit messages, while the other (the receiver) cannot send messages back—i.e., the sender receives no information from its partner. Two of the three agents are randomly selected and assigned as sender or receiver, and XP training is used. This setup reflects the unidirectionality typical of referential games.

Agents are evaluated under two conditions: *Normal* (scores sampled from $[2, 4, 6, \dots, 248]$) and *Hard* (scores sampled from $[160, 162, \dots, 240]$). The result is shown in Tab. S3. In the *Normal* condition, agents achieve a high SR of 0.829 because certain score configurations allow effective guessing. For instance, if the sender observes a low score of 32 and the receiver observes 232, the receiver infers that the sender sees 32 and can wait, while the sender correctly judges that its item is unlikely to be a target and searches for the other.

In the *Hard* condition, however, SR drops to chance level (0.508). Because all scores are moderate, agents cannot reliably infer whether their item is a target. This result underscores the importance of bidirectional communication for achieving high SR in the ScoreG game.

Table S3: Performance of three XP agents with **unidirectional communication** under different test conditions.

Test Condition	SR	Length
Normal	0.829 ± 0.022	5.166 ± 0.162
Hard	0.508 ± 0.011	5.934 ± 0.503

C.3 Ablation: No Cooperation

Table S4: Ablation study on non-cooperative tasks (*IndividualG*). We report average rewards for two agents and the average episode length (mean ± standard deviation) under three communication conditions.

Condition	**Avg. Reward (First Player)**	**Avg. Reward (Second Player)**	**Avg. Length**
Normal	1.770 ± 0.180	1.878 ± 0.194	13.762 ± 1.240
Ablate-Noise	1.822 ± 0.152	1.910 ± 0.171	13.300 ± 1.364
Ablate-Zero	1.740 ± 0.135	1.945 ± 0.179	13.148 ± 1.124

A leading hypothesis suggests that language, or communication more broadly, emerges because agents need to share their intentions or knowledge to cooperate effectively. To test this hypothesis, we design an additional experiment in which agents are embodied in the same environment but pursue individual goals (i.e., each agent separately picks up any items in the map). In this setting, there is no mutual incentive for agents to pick up the same item—in other words, shared intentionality is removed. We use the same neural network architecture and training regime (XP) as in the *ScoreG* experiments. Agents can still send and receive messages from their partners, but we hypothesize that communication will be less useful because coordination is not required to achieve shared rewards. We describe this environment, called *IndividualG*, below.

IndividualG The game structure is similar to *ScoreG*, with agents placed in a 6×6 grid world and sharing the same action space. However, there are several key differences. First, no scores are assigned to items, and each item requires only a single agent to pick it up. Consequently, no shared reward is available to cooperative agents, and communication is unnecessary to succeed. Second, an agent receives a reward of +1 for each item it successfully collects. Items cannot be picked up by two agents simultaneously. There are four items in total, so the maximum reward for a single agent is 4. The Nash equilibrium is for each agent to pick up two items. The game ends after 20 time steps or once all items have been collected.

Results The goal of this experiment is to test whether communication is useful in non-cooperative tasks. In other words, can meaningful communication still emerge when cooperation is unnecessary?

We train three XP agents and evaluate them under three conditions: *Normal*, *Ablate-Zero*, and *Ablate-Noise*. In *Ablate-Zero*, agents' messages are replaced with zero tokens, preventing the transmission of meaningful signals. In *Ablate-Noise*, agents' messages are replaced with random samples drawn from a uniform distribution instead of the policy's output distribution. This setup forces agents to misinterpret their partners' messages if the communication learned during training had any effect. In each episode, two of the three agents are randomly assigned as the **First Player** and **Second Player**. We report the average reward (corresponding to the average number of items collected per episode) for both players to test for potential asymmetries in their behavior. Results are shown in Tab. S4. Across all three conditions, agents achieve similar performance, with no observable difference between the first and second players. This suggests that communication does not provide a measurable advantage when agents pursue independent rewards. In other words, without shared goals or incentives for coordination, the environment does not pressure agents to develop or rely on meaningful communication.

C.4 Analysis: Varying Vocabulary Size

In *ScoreG*, the agents typically complete the game in approximately 5-6 time steps because we introduce time pressure to encourage agents to finish the game as soon as possible. Varying the vocabulary size alters the capacity of information that can be conveyed through the message sequence. Here we train XP agents with $N_{\text{pop}} = 3$ with different vocabulary sizes. The default vocabulary size we used in the main text was 4 (i.e., $\mathbf{m_t} \in \{0, 1, 2, 3\}$). A smaller vocabulary should, in principle, encourage greater compositionality due to a smaller capacity.

As shown in Tab. S5, *topsim* remains relatively stable across vocabulary sizes of 4, 8, and 16. However, when the vocabulary size increases to 32, the *topsim* score drops to 0.25. The *repcom* scores, in contrast, do not follow this pattern. Although they lie within a narrow range, their means show a slight downward trend: the highest value occurs at a vocabulary size of 4 (1.692), and the lowest at 32 (1.566). Despite this monotonic decrease, the differences are small and the standard deviations overlap, indicating that *repcom* does not strongly align with the changes observed in *topsim*.

Table S5: **Ablation Study on Vocabulary Size.** Effect of vocabulary size on communication and performance metrics. Values are reported as mean ± standard deviation.

Vocab. Size	topsim	repcom	IC	Self-SR	Cross-SR
4	0.311 ± 0.111	1.692 ± 0.126	0.966 ± 0.017	0.939 ± 0.021	0.972 ± 0.004
8	0.352 ± 0.032	1.586 ± 0.084	0.902 ± 0.056	0.880 ± 0.057	0.975 ± 0.003
16	0.309 ± 0.052	1.634 ± 0.089	0.954 ± 0.030	0.933 ± 0.030	0.978 ± 0.001
32	0.251 ± 0.034	1.566 ± 0.075	0.954 ± 0.031	0.931 ± 0.031	0.977 ± 0.001

C.5 Generalization to Unseen Positions

We study how well communication generalizes when it comes to unseen object positions. We trained three XP agents to perform the ScoreG task on 17 food locations in a 5×5 grid and evaluated their generalization to 8 unseen locations. Train and test food locations are randomly selected.

Emergent language generalizes to unseen spatial configurations. We ask whether the emergent language developed by the agents supports reference to positions that were never observed during training. If messages encode spatial information in a systematic way, a linear classifier should be able to decode unseen positions from message embeddings. Following the decoding analysis in the main text, we train linear models to predict each component of the item state—score, vertical position, and horizontal position. As shown in Fig. S9, all three components can be decoded with above-chance accuracy from the agents' messages. Moreover, message embeddings are more linearly decodable than the raw token sequences, suggesting that the learned communication protocol captures spatial structure in a manner that supports extrapolation.

Agent coordination degrades under unseen spatial configurations. Despite the decodability results, coordination is noticeably weaker when agents face positions they have not previously encountered. As shown in Tab. S6, agents with communication achieve a success rate of 0.953 on seen locations, but performance drops to 0.756 on unseen locations. This indicates that, while the emergent language captures some spatial regularities, the resulting behavior does not fully generalize to novel configurations and relies partly on the distribution of positions observed during training.

Our hypothesis is that the degradation in performance comes from a non-robust coordination strategy rather than from an emergent language that fails to encode the relevant information. To isolate this, we train three XP agents that have full access to all item scores and to each other's observations but are not allowed to communicate, essentially a standard MARL setting without communication. The agents are trained on 17 item locations and tested on 8 unseen locations. As shown in Tab. S7, their success rate drops from 0.981 to 0.823, indicating that the generalization gap arises largely from the inherent limits of the MARL algorithm rather than from communication alone. Improving multi-agent generalization to unseen spatial configurations is an important challenge for both MARL and emergent communication research, but addressing it is beyond the scope of the present work.

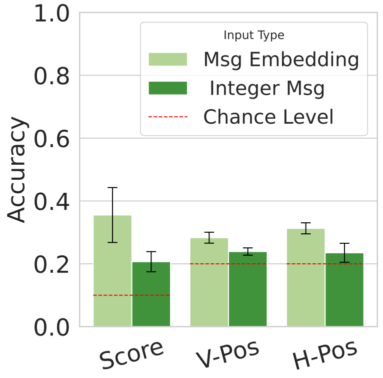

Figure S9: **Decoding unseen item states from messages.** *V-Pos*/*H-Pos* are item positions and *Score* is item value. *Integer Msg* uses raw message chains composed of integer sequences. *Msg Embedding* uses chained embeddings mapped from a lookup table. Error bars show standard deviations.

Table S6: Performance of three XP agents with communication on seen vs unseen locations.

Location	SR	Length
Seen	0.953 ± 0.017	5.197 ± 0.099
Unseen	0.756 ± 0.022	5.154 ± 0.229

Table S7: Performance of three XP agents without communication on seen vs unseen locations.

Location	SR	Length
Seen	0.981 ± 0.006	4.389 ± 0.038
Unseen	0.823 ± 0.023	4.092 ± 0.062

C.6 Analysis of Below-Chance Success Rates in Implicit Communication

In *Inv-NoCom* setting, the success rate (SR) falls below the chance level (See Fig. 5a), which indicates a systematic coordination failure rather than random performance. To better understand this phenomenon, we conduct two analyses: (i) ablation of the speed reward, and (ii) categorization of failure outcomes.

Ablation of the speed reward. The speed reward encourages efficient task completion. Removing this reward does not substantially change SR, which remains below chance. However, the absence of the speed reward increases the average episode length (Table S8). This result shows that the speed reward primarily affects efficiency but does not resolve the core coordination issue that leads to low SR.

Table S8: Effect of the speed reward on success rate (SR) and average episode length.

Reward Condition	SR	Length
With speed reward	0.438	5.607
Without speed reward	0.446	7.950

Failure outcome statistics. To diagnose why agents fail, we categorize episode outcomes into three groups: *correct pickups*, *wrong pickups*, and *no pickups*. Table S9 shows the distribution. Failures are dominated by wrong pickups (34.8%), followed by cases where agents never pick up the same item (27.4%). Together, these account for the below-chance success rate and show that agents struggle to coordinate reliably without communication.

Table S9: Distribution of episode outcomes without the speed reward.

Outcome	Percentage
Success: Correct Pickup	37.8%
Failed: Wrong Pickup	34.8%
Failed: No Pickup	27.4%

Overall, these findings show that below-chance SR in *Inv-NoCom* setting does not result from the speed reward but from miscoordination, most prominently through wrong item pickups.

C.7 ScoreG: Bumping and Cell Occupancy

Each grid cell can be occupied by at most one entity (either an agent or an item) at any given time. If an agent attempts to move into a cell that is already occupied by another agent, the move is blocked and the agent remains in its original position. We refer to such blocked moves as *bumping events*.

Although bumping could theoretically provide a minimal form of implicit communication (e.g., signaling another agent's location), it constitutes only a very low-bandwidth channel and becomes difficult to coordinate once agents are spatially separated. In practice, bumping is rare and therefore does not play a substantive role in coordination or communication. Tab. S10 summarizes the average number of bumps observed per episode across different conditions.

Table S10: Average bumps per episode.

Condition	Success	Failed
Inv-Com	0.179	0.065
Inv-NoCom	0.043	0.057
Vis-NoCom	0.015	0.020

These results confirm that while bumping exists as an artifact of the grid-world dynamics, it is too infrequent ($<$ 1 bump per episode) to support reliable strategies or emergent communication.

C.8 Positional Disentanglement

Topographic Similarity (*topsim*), while the most widely used metric in emergent language literature, is not the perfect measure for compositionality. (Chaabouni et al., 2020) introduced an alternative approach, measuring compositionality using disentanglement scores (Higgins et al., 2017). Specifically, **Positional Disentanglement (*posdis*)** (Chaabouni et al., 2020) quantifies how uniquely each message position encodes a single attribute, measuring the mutual-information gap

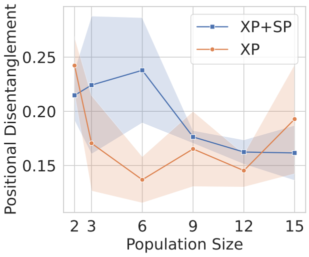

Figure S10: Positional Disentanglement *posdis* as a function of population size.

between its most and second most informative attributes. *posdis* could be used to measure another aspect of compositionality in our environment because this measure requires attributes to be discrete variables.

We conduct an experiment examining the relatioship between *posdis* and population size. Data for calculating *posdis* is collected and processed in the same way as *topsim*. Specifically, the message vector consists of a sequence of integers (tokens) and the attribute vector contains the item's score and position observed by a particular agent (See Sec. A.3). The result is shown in Fig. S10. In contrast to *topsim* trend for XP+SP agents, *posdis* decreases with population size. We observe a parabola-like curve for XP agents, peaking at sizes 3 and 15.

It is important to note that low *posdis* does not necessarily imply low overall language compositionality. This is because *posdis* is a very strict form of compositionality where a position in a message uniquely refers to a particular attribute. This condition does not hold if we use the position of the character level. The stringency of *posdis* condition limits its general applicability.

D TemporalG: Additional Results and Analyses

Table S11: Performance of XP agents in the 5×5 *TemporalG* environment with the fixed duration of 6. N_{pop}: population size. LS: language similarity; Cross-SR: success rate with other agents; Self-SR: success rate in self-play. All values are reported as mean ± standard deviation across held-out agent pairs.

Model	N_{pop}	**LS**	**Cross-SR**	**Self-SR**
XP	3	0.336 ± 0.012	0.975 ± 0.003	0.962 ± 0.006

D.1 Implicit Communication

As shown in Tab. S12, three XP agents trained without communication under the invisible-partner condition (*Inv-NoCom*) still achieved relatively high success at a fixed duration of 6, likely by adopting a waiting strategy—that is, delaying movement to infer the spawn order. Their longer episode lengths, compared to the other two conditions (*Inv-Com* and *Vis-NoCom*), support this interpretation. However, when the fixed duration was increased, the number of possible spawn times doubled (from 6 to 12), rendering the waiting strategy ineffective and causing the success rate of *Inv-NoCom* agents to fall below chance level. Similar to what was observed in *ScoreG* experiment in Sec. 5, *Vis-NoCom* agents achieved performance comparable to *Inv-Com*, suggesting that they exploited visual cues for implicit coordination, especially under the limited set of six possible spawn times. In the *Inv-Com-Noise* condition, agents were trained with explicit communication but tested without it (messages were always zero). The low SR observed in this condition implies that meaningful messages are necessary for agents trained with communication (*Inv-Com*) to succeed at the task.

Table S12: Implicit communication in the 8×8 *TemporalG* with fixed durations of 6 and 12. Length denotes the average length of successful episodes (not applicable in the bottom-right cell, where some runs yielded zero successes). Abbreviations are the same as those reported in Fig. 5.

Condition	Fixed Duration = 6		Fixed Duration = 12	
	SR	Length	SR	Length
Inv-Com	0.980 ± 0.035	23.990 ± 0.618	0.961 ± 0.021	30.023 ± 0.775
Inv-NoCom	0.728 ± 0.155	28.716 ± 2.341	0.419 ± 0.137	31.738 ± 1.780
Vis-NoCom	0.939 ± 0.093	24.516 ± 0.307	0.862 ± 0.110	30.546 ± 0.406
Inv-Com-Noise	0.313 ± 0.040	28.666 ± 0.774	0.003 ± 0.001	—

D.2 Rendezvous Behavior Analysis

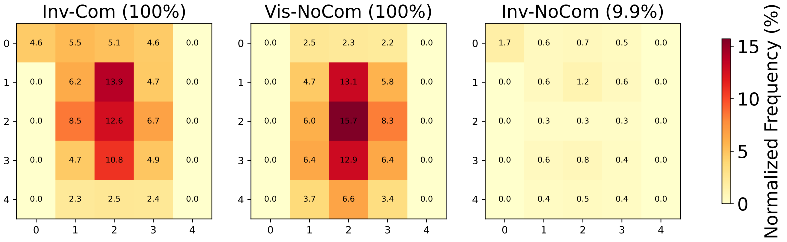

Figure S11: Rendezvous maps of first meeting points across conditions. Values represent normalized frequencies of encounters on the 5×5 grid. *Inv-Com* and *Vis-NoCom* agents consistently meet and converge near the center, while *Inv-NoCom* agents rarely meet and show no strong central bias.

Restricting the communication range forces agents to meet in physical proximity before they can exchange information. This environmental constraint gives rise to rendezvous points: locations where agents repeatedly converge to initiate communication. Despite this restriction, displacement remains necessary. Agents must explore the grid to observe items, store these observations in memory, and then communicate the information once they encounter their partner. Since neither agent can directly infer when all items have appeared without exchanging messages, coordination still relies on communication.

To analyze where meetings occur, we compute a rendezvous map that records the normalized frequency of the first meeting location across episodes. The resulting heatmaps reveal a pronounced central bias: agents overwhelmingly converge near the middle of the 5×5 grid (See Fig. S11). This bias emerges because the center minimizes travel distance and maximizes the probability of encounter under partial observability.

When comparing conditions, clear differences emerge. *Inv-Com* agents always meet (100% of episodes) and almost exclusively converge in the central cells, reflecting highly coordinated rendezvous behavior. *Vis-NoCom* agents also meet in every episode, showing a similar central bias, suggesting that visibility supports coordination even without explicit messages. By contrast, *Inv-NoCom* agents succeed in meeting in only 9.9% of episodes, and when they do meet, the rendezvous points are weakly defined and scattered across the grid.

E PPO WITH RECURRENT MEMORY TRANSFORMER

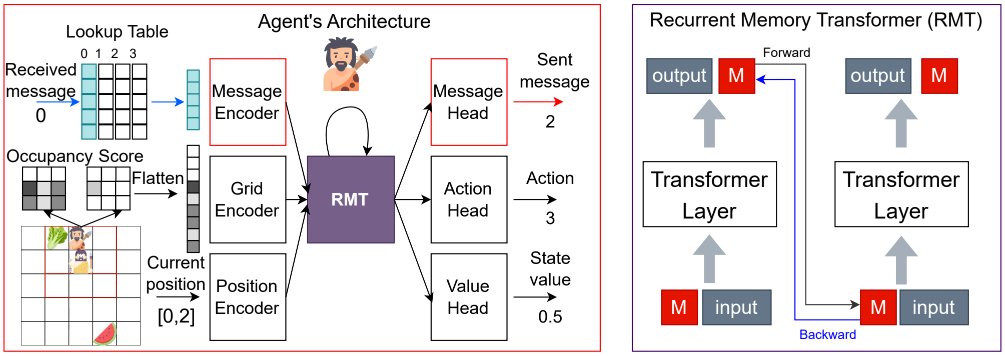

Figure S12: **PPO-RMT Architecture:** RMT can serve as a direct replacement for a traditional RNN in standard RL architectures, since it fulfills the same recurrent role. The memory token (M) functions analogously to an RNN's hidden state and provides a mechanism for backpropagation through time (BPTT).

E.1 ARCHITECTURE

The agent uses the same input encoders as in the original architecture Fig. S12), but replaces the LSTM core with a tiny GPT-style Recurrent Memory Transformer (RMT) (Bulatov et al., 2022; 2024) that operates over a pair of tokens: a memory token and a current observation token. As before, the encoders map heterogeneous inputs into a common feature space, while the output heads map the resulting latent representation to the outgoing message, action, and value prediction.

On the input side, we retain the message encoder $\mathcal{E}_{\mathcal{M}}$, grid encoder $\mathcal{E}_{\mathcal{X}}$, and position encoder $\mathcal{E}_{\mathcal{P}}$. Given at time step t the incoming message m_t, the grid observation x_t, and the agent's position p_t, the encoders produce feature vectors

$$e_t^{\mathcal{M}} = \mathcal{E}_{\mathcal{M}}(m_t) \in \mathbb{R}^{d_{\mathcal{M}}}, \qquad e_t^{\mathcal{X}} = \mathcal{E}_{\mathcal{X}}(x_t) \in \mathbb{R}^{d_{\mathcal{X}}}, \qquad e_t^{\mathcal{P}} = \mathcal{E}_{\mathcal{P}}(p_t) \in \mathbb{R}^{d_{\mathcal{P}}}.$$

All encoders are implemented as shallow MLPs; $\mathcal{E}_{\mathcal{M}}$ includes an embedding layer that maps each vocabulary index to a dense vector before applying the MLP. These features are concatenated,

$$z_t = [\, e_t^{\mathcal{X}};\, e_t^{\mathcal{P}};\, e_t^{\mathcal{M}} \,] \in \mathbb{R}^{d_{\text{in}}},$$

and projected into the transformer model dimension d_{model} using a learned linear projection,

$$o_t = W_{\text{in}} z_t + b_{\text{in}} \in \mathbb{R}^{d_{\text{model}}}.$$

The agent maintains a recurrent memory state $h_{t-1} \in \mathbb{R}^{d_{\text{model}}}$, initialized to zero at the beginning of each episode. Instead of feeding (z_t, h_{t-1}) into an LSTM, the PPO-RMT constructs two tokens:

$$m_t = W_{\text{mem}} h_{t-1} + b_{\text{mem}} \in \mathbb{R}^{d_{\text{model}}}, \qquad o_t \in \mathbb{R}^{d_{\text{model}}},$$

and stacks them into a length-2 sequence,

$$X_t^{(0)} = \begin{bmatrix} m_t \\ o_t \end{bmatrix} \in \mathbb{R}^{2 \times d_{\text{model}}}.$$

This 2-token sequence is processed by a stack of L transformer blocks $\{\mathcal{F}^{(\ell)}\}_{\ell=1}^{L}$, each consisting of multi-head self-attention followed by a feedforward MLP, both wrapped in residual connections and layer normalization. Given an input $X \in \mathbb{R}^{2\times d_{\text{model}}}$, each block performs:

$$\begin{aligned}\tilde{X} &= \mathrm{LN}_1(X),\\ H &= \mathrm{MHSA}(\tilde{X}),\\ X' &= X + H,\\ \hat{X} &= \mathrm{LN}_2(X'),\\ G &= \mathrm{MLP}(\hat{X}),\\ X^{\text{out}} &= X' + G.\end{aligned}$$

The multi-head self-attention over the two tokens is defined as follows. For each head $i = 1, \dots, H$,

$$Q_i = XW_i^Q, \qquad K_i = XW_i^K, \qquad V_i = XW_i^V,$$

with $W_i^Q, W_i^K, W_i^V \in \mathbb{R}^{d_{\text{model}}\times d_k}$, and

$$\mathrm{Attn}_i(X) = \mathrm{softmax}\left(\frac{Q_i K_i^\top}{\sqrt{d_k}}\right) V_i \in \mathbb{R}^{2\times d_v}.$$

The per-head results are concatenated and projected:

$$\mathrm{MHSA}(X) = \big[\mathrm{Attn}_1(X); \dots ; \mathrm{Attn}_H(X)\big] W^O,$$

with $W^O \in \mathbb{R}^{(Hd_v)\times d_{\text{model}}}$. Because the sequence length is fixed at exactly two tokens, the transformer effectively learns how to mix and combine information between the memory token and the observation token, creating a learned recurrent update. After passing through all L blocks, we obtain:

$$X_t^{(L)} = \begin{bmatrix} h_t^0 \\ h_t^1 \end{bmatrix} \in \mathbb{R}^{2\times d_{\text{model}}}.$$

We take the second token as both the output representation and the next-step memory state:

$$\tilde{h}_t = h_t^1 \in \mathbb{R}^{d_{\text{model}}}.$$

At episode boundaries, memory is reset using the done flag, following the implementation of LSTM by Huang et al. (2022), $d_t \in \{0, 1\}$:

$$\tilde{h}_t \leftarrow (1 - d_t)\, \tilde{h}_t.$$

On the output side, the same three heads as in the PPO-LSTM architecture operate on the transformer hidden state h_t. Thus, relative to the PPO-LSTM agent, the only architectural change lies in the recurrent core: instead of an LSTM's gated updates, the PPO-RMT performs a learned recurrence via self-attention over a fixed pair of tokens representing the previous memory and the current observation.

E.2 Results

Table S13: **Performance and language statistics for PPO-RMT.** Values are reported as mean ± standard deviation.

Model	N_{pop}	**Self-SR**	**Cross-SR**	**IC**	**LS**
XP	2	0.400 ± 0.121	0.951 ± 0.000	0.420 ± 0.127	0.354 ± 0.036
XP+SP	2	0.953 ± 0.003	0.951 ± 0.005	1.002 ± 0.002	0.636 ± 0.020
XP	3	0.939 ± 0.009	0.942 ± 0.007	0.997 ± 0.002	0.631 ± 0.024

We conduct experiments in *ScoreG*. and compare the results with PPO-LSTM. The first part is a qualitative comparison, showing that self-play and population training can lead to a shared, interchangeable language. The second part is comparing cultural transmission performance between PPO-LSTM and PPO-RMT.

PPO-RMT agents show that self-play and larger populations improve language interchangeability. Across conditions, XP agents display low *Self-SR* (0.40 ± 0.12) despite strong

Cross-SR, indicating poor interchangeability and low *LS*. Adding self-play (XP+SP) substantially improves performance, yielding high *Self-SR* (0.953 ± 0.003), stable *Cross-SR*, and increased *LS*. Increasing the population size without self-play (XP with $N_{\text{pop}} = 3$) similarly enhances language consistency and interchangeability, achieving high *Self-SR* (0.939 ± 0.009) and strong *LS*. Overall, both self-play and larger populations support more consistent and interchangeable communication in PPO-RMT agents.

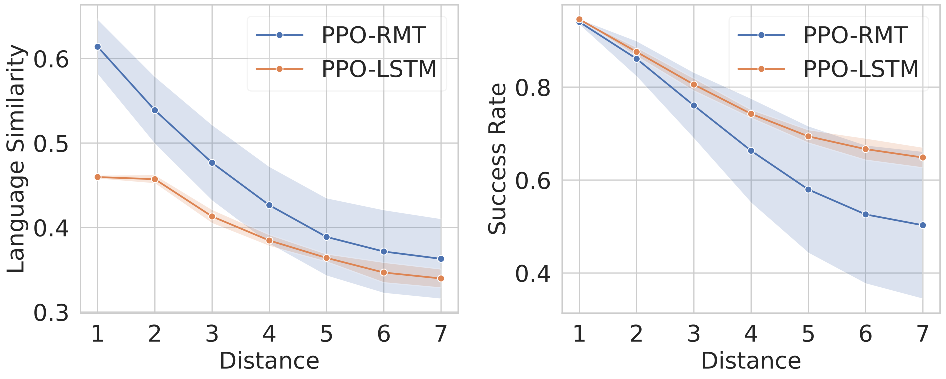

(a) *LS*

(b) *SR*

Figure S13: **PPO-RMT vs. PPO-LSTM trained with XP+SP under a Ring Social Network.** (a) Language Similarity (*LS*) across social distances. (b) Success Rate (*SR*) across social distances. Shaded areas denote standard deviations across 3 training seeds.

PPO-RMT exhibits larger variance in LS and SR than PPO-LSTM. As shown in Fig. S13, both PPO-LSTM and PPO-RMT trained with XP+SP display gradually decreasing *LS* and *SR* as social distance increases, indicating that self-play facilitates cultural transmission to non-partner (unseen) agents. However, PPO-RMT shows noticeably higher variance in both *LS* and *SR*, suggesting that cultural transmission under PPO-RMT is less stable and more sensitive to training seeds compared to PPO-LSTM.

F A New Challenge: Procedurally Generated Task

Language can be used to solve increasingly complex tasks, not only simple ones. In this section, we scale up the tasks by adding random walls during training, resulting in more diverse layouts, inspired by the environment proposed in Samvelyan et al. (2023).

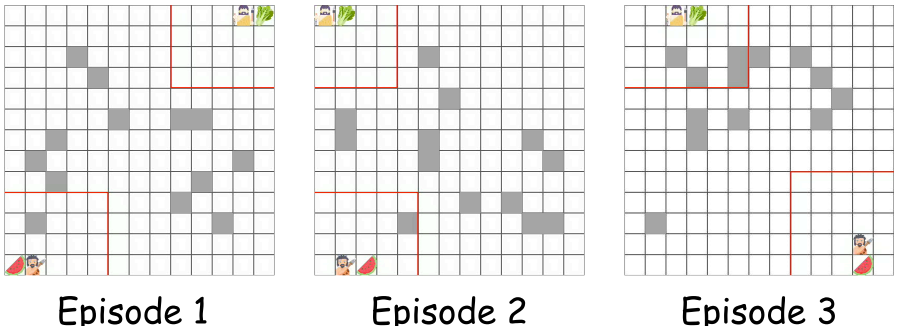

Figure S14: **Examples of *ScoreG-Scale* episodes at the most complex stage**: 13 walls are placed randomly across 99 cells, resulting in 6 quadrillion unique layouts, impossible for agents to see all of them. Communication range is also limited.

Environment Structure: We propose *ScoreG-Scale*, which shares the same transition dynamic and goal as in the original *ScoreG*. In this task, agents are in a 13×13 grid world and have a receptive field with size 7×7. The communication range is limited within 7×7 cells centered at the agent position. In other words, agents can successfully send a message if they are in each other's visual field. We make agents blind to each other so they cannot rely on additional information not contained in messages. Additionally, 13 walls can be randomly placed in 9×11 cells around the center cell. This results in 6 quadrillion (6×10^{15}) unique environment layouts. We set the maximum time steps per episode (episode length) to be 30.

Curriculum Training: Training agents from scratch in this complex environment is impractical. We manually design curricula for agents to learn to make the convergence easier. We gradually add difficulty to the task. The first thing to vary is the initial positions. There are three stages of initial positions. First, agents are placed on one end (top or bottom) near each other along with their corresponding items. Intuitively, agents can learn to communicate more at this stage as the task is easy to accomplish. Second, one agent is placed in the top or bottom row, and another agent is placed in the middle row. Third, one agent is placed on either the top or bottom row, and another agent is placed on the opposite (top or bottom) side of the first one. The number of walls increases from zero (no wall) linearly with the environment steps and reaches the maximum at 90% of the total environment steps used for training. At late training, the task is more challenging as the agents have to adjust their strategy to navigate and pick up the goal item. We remove the bonus reward as agent time steps can vary depending on task difficulty; therefore, the maximum return is 1, i.e. return implies success rate.

Results: We train two models on the more complex task mentioned above. The first model has 200k parameters, which is the one we use in all other experiments. To study if scaling up the model really benefits solving more complex tasks, we increase the hidden dimension of the LSTM layer from 128 to 4096, resulting in 67M parameters, which is 335 times bigger than the first one. In the early training, the task is easy; we do not see any difference between the two models. However, when the complexity increases, we observe performance degradation of the big model, likely because bigger models tend to be more overfitting. It is not surprising that naively scaling up the model size does not improve the learning. Actually, it is preferable for the RL model to be small (e.g., less than 30M). This is probably because RL problems are inherently serial, as theorized by Liu et al. (2025b), and parallel scaling may not greatly improve learning as reported by Wang et al. (2025b).

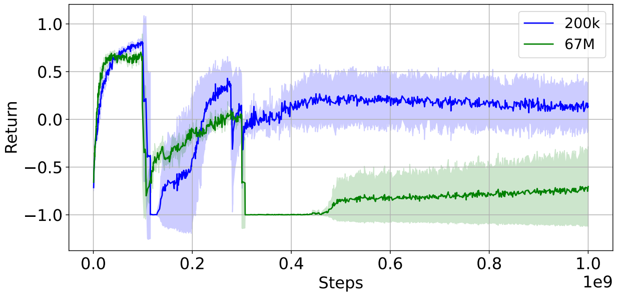

Figure S15: **Learning performance on procedurally generated *ScoreG-Scale***: 200k refers to the default model used in the main text with 200k parameters and 67M refers to the scaled up model with 67M parameters.